STABLE TEARING CHARACTERIZATION OF THREE MATERIALS WITH THREE METHODS

by

ELIZABETH NICOLE JOHNSTON

B.A., Kansas State University, 2008

A THESIS

submitted in partial fulfillment of the requirements for the degree

MASTER OF SCIENCE

Department of Mechanical and Nuclear Engineering
College of Engineering

KANSAS STATE UNIVERSITY
Manhattan, Kansas

2012

Approved by:

Major Professor
Dr. Kevin Lease

Copyright

Abstract

Over the past several years the crack tip opening angle (CTOA) has been identified as one of the key fracture parameters to characterize low constraint stable tearing and instability in structural metallic alloys. This document presents the results of experimental stable tearing characterizations. Characterization methods include optical microscopy and marker band measurements of crack front tunneling. Specific attention is given to the measurement methods used, and also the correlation between CTOA and Delta-5. The effect of tunneling and comparisons with computational results are discussed, and the effect of material and measurement method on CTOA is observed and a clear relationship is seen. Preliminary work on future studies into internal features and behavior is also presented.

Table of Contents

List of Figures vi

List of Tables viii

Acknowledgements ix

Dedication x

Chapter 1 – Introduction 1

Background 1

Extension and Application of CTOA 2

Key Results 3

Framework for Thesis 5

References 6

Chapter 2 – CTOA Measurement Methods and Crack Tunneling in 2024-T351 Aluminum Alloy 11

Chapter 3 – Multiple-Method CTOA Stable Tearing Characterization of Three Metallic Alloys 12

Introduction 13

CTOA Measurement Methods 14

CTOA Measurement Method 1 16

CTOA Measurement Method 2 17

CTOA Measurement Method 3 18

Experimental CTOA Results 19

Material Behavior 20

Material and Method Effect on Initial CTOA-Δa Behavior 21

Experimental Critical CTOA 24

Measurement of δ_5 28

Experimental δ_5 Results 28
Overall δ_5 R-curve Behavior 28
CTOA-Δa and Critical CTOA from δ_5 R-curve 29
Discussion 32
References 36
Chapter 4 – Additional Developments 39
Introduction 39
Material Selection 40
Specimen Geometry Selection 40
Stable Tearing Characterization 41
CTOA Measurement 42
Tunneling Measurement 45
Preparation for APS 47
References 48
Chapter 5 – Conclusion 50

List of Figures

Figure 1.1: Definition of CTOA and CTOD a fixed distance behind the crack tip 1

Figure 3.1: Overview of CTOA parameter: (a) illustration of how CTOA is defined, and (b) example CTOA data showing initial high region dropping to lower, constant region 13
Figure 3.2: Illustration of the three general "ranges" used in the three measurement methods ... 14
Figure 3.3: Illustration of the defined phases that the crack flanks experience as the measurement ranges follow the progressing surface crack tip 15
Figure 3.4: Idealized trends for each method in the initial non-constant CTOA region (only the first several mm of surface crack extension). The x-axis is essentially the amount of surface crack extension, but is not to scale because the phases are shown instead 16
Figure 3.5: General illustration of the selection of points in the three "ranges" and how the CTOA is defined using the points, for (a) Method 1, (b) Method 2, and (c) Method 3 17
Figure 3.6: Flank shapes, due to fracture type, for the three materials in this study 20
Figure 3.7: Transitions from blunting pre-crack tip region to stable tearing crack region for all three materials in this study 21
Figure 3.8: Initial non-constant CTOA region for 2024-T351, with vertical lines indicating where each phase occurs 22
Figure 3.9: Initial non-constant CTOA region for 5083-H321 Al, with vertical lines indicating where each phase occurs 23
Figure 3.10: Initial non-constant CTOA region for Ti-6Al-4V, with vertical lines indicating where each phase occurs 24
Figure 3.11: Method 1 CTOA measurements for all materials in the current study [13] 25
Figure 3.12: Method 2 CTOA measurements for all materials in the current study [13] 26
Figure 3.13: Method 3 CTOA measurements for all materials in the current study [13] 26
Figure 3.14: R-curves for the δ_5 parameter for each material in this study [13] 29
Figure 3.15: CTOA-Δa curve from δ_5 data, compared to Method 1 results, for 2024-T351 Al... 30
Figure 3.16: CTOA-Δa curve from δ_5 data, compared to Method 1 results, for 5083-H321 Al .. 30
Figure 3.17: CTOA-Δa curve from δ_5 data, compared to Method 1 results, for Ti-6Al-4V 31

Figure 4.1: CTOA-Δa curves for Specimens 2 and 11 43
Figure 4.2: Load-Δa curves for Specimens 2 and 11 44
Figure 4.3: Fracture surface of Specimen 11, showing marker bands 46

List of Tables

Table 3.1: Comparison of experimental critical CTOA values obtained in the current study for multiple measurement methods and multiple materials [13] 27

Table 4.1: Critical CTOA and standard deviation results 43

Table 4.2: Marker band application parameters for Specimen 11 45

Acknowledgements

It would be negligent if I did not acknowledge those who have helped me immensely along this journey. First and foremost, acknowledgement and many thanks go to my major professor Dr. Kevin Lease. He has spent many hours editing and providing suggestions on my thesis chapters. He has helped me to grow as a researcher and as a professional member of society. I would not be here without his initial faith in my abilities and many opportunities to grow.

Second, I must thank my fiancé, Josh Johnston. He has helped to keep me focused on the prize the last many months. It is with his encouragement that I continue on to finish the PhD that I have started.

My parents also deserve thanks for the many years of support that they provided to me at home, and the continued support that they gave me after I left home and ventured into first undergraduate work, then into graduate work. Without my parents' support, I would have lost focus during my undergraduate studies and pursued firefighting. My sister has also provided support by being interested in my research and by providing my sanity break during the first two years of my graduate studies.

I also acknowledge the Mechanical and Nuclear Engineering Department, for their resources and wonderful staff. Eric Wagner, director of the ME shop (and Jason Selland, former shop director), provided services and guidance necessary for obtaining many special fixtures and specimens for my experimental work.

Dedication

This thesis is dedicated to my grandfather, Robert Frink, who was also a Mechanical Engineering graduate (from Rensselaer Polytechnic Institute). Although I never knew him, I must have taken after him in some ways. I wish he were here to compare notes.

Chapter 1 – Introduction

Background

Low constraint conditions occur in specimens having large in-plane dimensions as compared to thickness. Stable crack extension (stable tearing) is a fracture phenomenon that occurs in these low constraint conditions with large amounts of contained plasticity at the crack tip. The resistance to this phenomenon has been characterized using several candidate parameters including crack tip stress or strain, crack-tip-opening displacement or angle, crack tip force, energy release rates, J-integral, and tearing modulus. The crack-tip-opening angle (CTOA) or displacement (CTOD) at a specified distance (d) from the crack tip (see Figure 1.1 – relationship easily derived) was shown to be the most promising for modeling stable crack growth and instability during the fracture process [1-4].

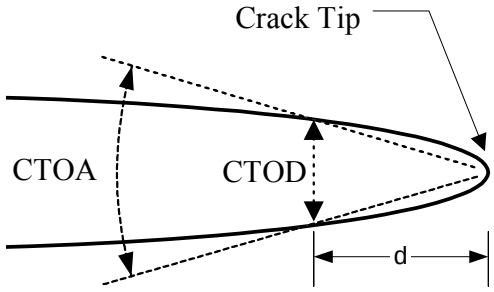

Figure 1.1: Definition of CTOA and CTOD a fixed distance behind the crack tip

The general failure process for a metallic material that undergoes large amounts of plastic deformation near a pre-existing sharp crack (fatigue crack, stress-corrosion crack, etc.) in low constraint conditions has been shown to consist of three distinct phases: (1) crack blunting/ initiation, (2) stable crack extension, (3) unstable crack extension after maximum load carrying capacity is reached. Low constraint conditions occur when the thickness of the specimen is such that plane stress predominates (this occurs in thin specimens). A plane strain core exists at the mid-thickness, and the size of the core depends on the thickness of the specimen and the material. In plane stress conditions, there are no out-of-plane stress components but there can be significant out-of-plane deformation. In plane stress conditions the material behaves with a significant amount of plasticity. In plane strain conditions, stresses are triaxial and the material behaves brittle-like, with little yielding, thus less fracture resistance than the plane stress conditions at the surface of the specimen. Because of the differences in state-of-stress between the surface and the mid-thickness core, a crack tip will extend more easily in the plane strain core and the crack tip at the surface will lag behind, due to the large amount of plasticity there.

Over the past several decades, in-depth studies of stable crack extension in metallic materials (mode I loading) have been performed using elastic-plastic finite element methods [1-12]. These studies focused on the simulation of stable initiation and stable extension while evaluating several local and global fracture criteria. However, one significant drawback is that a different experimental critical CTOA value is required for each thickness of material in order to predict stable crack growth, as the critical CTOA is dependent on the material thickness and crack-front constraint [13]. In these simulations, 3D finite element analysis, or a 2D finite element analysis with a plane strain core must be used. The size of the plane strain core is adjusted to match experimental data.

A variety of studies (computational and experimental) have focused on characterizing CTOA over its history. However, essentially none have attempted to study the internal features of the stable tearing phenomena (such as crack tunneling), especially at the very early stages (blunting/initiation/early tunneling). The few that studied the internal features used advanced computational techniques and/or tedious *post mortem* experimental techniques to attempt to capture internal behaviors.

Extension and Application of CTOA

Although early computational results from de Koning [1] showed that CTOA was nearly constant after crack initiation, Shih *et al* [2] and Kanninen *et al* [3] showed that the CTOA at initiation was larger than the value during stable crack growth. However, Newman [4] used a constant CTOD (or CTOA) value obtained from a laboratory compact specimen to model crack initiation, stable crack growth and instability, and predicted the failure loads on two other crack configurations within about 10 percent of experimental failure loads. In addition, other researchers [10-12] showed that the CTOA took on a nearly constant value after a small amount of stable crack extension for a variety of materials and thicknesses. Some of these discrepancies in the early finite-element based simulations of stable tearing using the CTOD/CTOA parameters have been attributed to using a simplified assumption of either plane stress or plane strain conditions at the crack tip, when the physics of the situation reveal that there is high-constraint and therefore high stress triaxiality at the crack tip – implying that 3D analyses would be required [14-16]. More recently, the finite-element method (a shell code - STAGS - and the plane-strain core) and the CTOA failure criterion has been successfully applied to some very

complex structural configurations with single or multiple cracks in flat and curved stiffened panels under severe out-of-plane deformations made of thin-sheet 2024 aluminum alloys [17-19]. A comparison of the experimental and predicted (STAGS) load vs. crack extension for a stiffened panel with a single center lead crack and 1.3 mm MSD, as well as the relative location of the lead crack, open holes, MSD and stiffener was performed by Seshadri, *et al* [18]. The results indicated that the elastic-plastic FEM analysis and the CTOA fracture criterion can predict stable tearing and residual strength in the presence of MSD in a complex stiffened panel with severe out-of-plane deformations, typical of what may occur in an aircraft fuselage under pressure.

Numerous investigators [20-33] have also experimentally measured CTOD or CTOA during the fracture process. The results of Luxmoore, *et al* [20] indicated that the constant CTOA (CTOD) value was dependent on specimen configuration. Experiments conducted by Schwalbe and Hellmann [22] correlated a modified CTOD parameter (δ_5 COD parameter) with crack extension data for various specimen types. Reuter *et al* [23], using microtopography to reconstruct the stable tearing process, found that CTOD was nearly linearly related to crack extension – implying a nearly constant CTOA during stable crack extension. Llyod and Piascik [24], using a fracture surface microtopography analysis system, measured CTOA on thin-sheet aluminum alloy and found that CTOA was nearly constant after the blunting process. Dawicke *et al* [25], using a high-resolution camera with a video system, showed the same results of a nearly constant (critical) CTOA after a small amount of crack extension. The non-constant CTOA region (measured at the free surface) was shown to be associated with severe tunneling (crack front at the surface lagging behind the crack front at the mid-plane) during the initiation of stable tearing.

Key Results

Dawicke and Sutton [26] have compared the high-resolution photographic method and a digital-imaging correlation method to measure the surface CTOA values. These two methods give very similar CTOA values on thin-sheet aluminum alloys. Mahmoud and Lease [27, 28], using these two experimental techniques, have measured surface CTOA values on aluminum alloys of various thicknesses. Comparing CTOA vs. crack extension results from Dawicke's work [26] on thin sheet 2024-T3 and Mahmoud and Lease's work [27, 28] on thick plate 2024-T351, the thick plate reached a constant value quicker than the thin sheet. It was also seen that for the thicker

specimens, the CTOA is once again nearly constant after a small amount of crack extension and remains constant over a wide range in thickness. In addition, the non-constant CTOA region and the scatter in measured CTOA values became smaller for the thicker specimens. Burton, *et al* [31] have developed a highly automated digital image based system for capturing and analyzing crack tip opening angle images during stable testing. This technique has been shown to provide enhanced ability in evaluating the early blunting/initiation phase of the stable tearing process. Burton, *et al* [32] showed that the constant CTOA approach can accurately simulate the load-crack extension behavior of the laboratory fracture specimens. Looking at the experimental and simulated load vs. crack extension response for 16 mm thick titanium C(T) specimens (W = 152 mm), Burton, *et al* [32] obtained three different curves representing three different levels of slant fracture behavior observed in the experimental results.

Recently, several researchers [34-40] have investigated the CTOA obtained from alternative methods of measuring the angle between the flanks near the crack tip. These methods were meant as a means to simplify the measurement process by eliminating the need to accurately locate the crack tip. In addition, a study of alternative methods by Burton, *et al* [31] indicates that variation of the measurement method and/or the placement of the measurements relative to the crack tip can have a marked effect on the behavior of the CTOA resistance curve as well as the critical CTOA value. This introduces propagation of error in the prediction of stable crack growth.

The tunneling phenomenon has been an issue of interest in several researchers' studies [15, 34, 41-45], but with limited progress in literature towards predicting tunneling [46]. By applying fatigue marker bands, but then utilizing the resulting crack front shapes in a three-dimensional, elastic-plastic, finite-element analysis code (ZIP3D [47]), Dawicke, *et al* [15] showed that the CTOA through the thickness varied significantly during the initial 3 mm of surface crack extension but then approached a similar, constant value through the thickness after 3 mm of extension (for 2.3 mm thick M(T)). During the initial 3 mm of surface crack extension, the results indicated that CTOA was lower at the mid-plane (due to high constraint [45]) and higher at the surface. James and Johnston [48] have investigated tunneling and the CTOA through-the-thickness, but measuring normal to the crack front rather than parallel to the overall direction of crack growth. Their results for surface and interior angles computationally obtained normal to

the crack front, show that the CTOA reaches a near constant value quite quickly, relative to the thickness of the specimens (~2.5 mm vs. 6.35 mm).

It should be noted that three-dimensional, elastic-plastic, finite-element analysis simulations using the critical CTOA criterion are known to over-predict the amount of surface crack extension. This is commonly attributed to the simplicity of the critical CTOA criterion, the transition from flat to slant fracture after maximum load, and the tunneling phenomenon combined with the fact that finite-element codes use mid-plane nodal release, thus corresponding with the crack front at the mid-plane of the specimen rather than at the surface where experimental critical CTOA and crack extension were measured [13, 42, 44, 49].

Framework for Thesis

This thesis will present work in the form of two journal manuscripts (one chapter each) with a third chapter containing recent work. The first manuscript (Chapter 2) discusses various CTOA measurement methods employed on 2024-T351 Al, as well as an investigation of tunneling and an "apparent crack tip" determined from the various measurement methods. The effect of tunneling on load vs. crack extension (load-Δa) curves from computational studies vs. experimental studies is described as well. The second manuscript (Chapter 3) discusses various CTOA measurements employed on three materials, to further expand the understanding of the CTOA measurement methods used in Chapter 2. Relationships between the measurement methods, materials and CTOA-Δa curve are also discussed. The additional work chapter (Chapter 4) describes recent work performed to transition from investigations of the surface (as in Chapters 2 and 3) to investigations of internal aspects. In addition, synchrotron-based methods are suggested and preparations for these methods are discussed. Finally, Chapter 5 will present overall conclusions from this work.

References

1. de Koning, A. U., "A Contribution to the Analysis of Slow Stable Crack Growth,", National Aerospace Laboratory Report NLR MP 75035U, 1975.
2. Shih, C F., de Lorenzi, H. G. and Andrews, W. R., "Studies on Crack Initiation and Stable Crack Growth," ASTM STP 668, 1979, pp. 65-120.
3. Kanninen, M. F., Rybicji, E. F., Stonesifer, R. B., Broek, D., Rosenfield, A. R. and Nalin, G. T., "Elastic-Plastic Fracture Mechanics for Two-Dimensional Stable Crack Growth and Instability Problems," ASTM STP 668, 1979, pp. 121-150.
4. Newman, J. C., Jr., "An Elastic-Plastic Finite Element Analysis of Crack Initiation, Stable Crack Growth, and Instability," ASTM STP 833, 1984, pp. 93-117.
5. Kobayashi, A. S., Chiu, S. T. and Beeuwkes, R., "A Numerical and Experimental Investigation on the Use of the J-Integral," Engineering Fracture Mechanics, Vol. 5, No. 2, 1973, pp. 293-305.
6. Anderson, H., "A Finite-Element Representation of Stable Crack Growth, Journal of Mechanics and Physics of Solids," Vol. 21, 1973, pp. 337-356.
7. Light, M. F., Luxmoore, A. and Evans, W. T., "Prediction of Slow Crack Growth by a Finite Element Method," International Journal of Fatigue, Vol. 11, 1975, pp. 1045-1046.
8. Newman, J. C., Jr., "Finite Element Analysis of Crack Growth Under Monotonic and Cyclic Loading," ASTM STP 637, 1977, pp. 56-80.
9. Rousselier, G., "A Numerical Approach for Stable-Crack-Growth and Fracture Criteria," Fourth International Conference on Fracture, Canada, Vol. 3, 1977.
10. Brocks, W. and Yuan, H., "Numerical Studies on Stable Crack Growth," ESIS/EGF9 (Edited by J. G. Blauel and K.-H. Schwalbe), Mechanical Publications, London, 1991, pp. 19-33.
11. Newman, J. C., Jr., Shivakumar, K. N. and McCabe, D. E., "Finite Element Fracture Simulation of A533B Steel Sheet Specimens," ESIS/EGF9 (Edited by J. G. Blauel and K.-H. Schwalbe), Mechanical Publications, London, 1991, pp. 117-126.

12. Demofonti, G. and Rizzi, L., "Experimental Evaluation of CTOA in Controlling Unstable Ductile Fracture Propagation," ESIS/EGF9 (Edited by J. G. Blauel and K.-H. Schwalbe), Mechanical Publications, London, 1991, pp. 693-703.

13. Newman Jr., J.C. and James, M.A., "A Review of the CTOA/CTOD Fracture Criterion – Why it Works!" AIAA-2001-1324, pp. 1042-1051.

14. Newman, J. C., Jr., Booth, B. C. and Shivakumar, K. N., "An Elastic-Plastic Finite-Element Analysis of the J-Resistance Curve using a CTOD Criterion," ASTM STP 945, 1988, pp. 665-685.

15. Dawicke, D. S., Newman, J. C., Jr. and Bigelow, C. A., "Three-Dimensional CTOA and Constraint Effects during Stable Tearing in a Thin-Sheet Material," ASTM STP 1256, 1995, pp. 223-242. (Same as NASA TM 109183, February 1995)

16. Gullerud, A. S., Dodds, R. H., Jr., Hampton, R. W. and Dawicke, D. S., "Three-Dimensional Modeling of Ductile Crack Growth in Thin Sheet Metals: Computational Aspects and Validation," Engineering Fracture Mechanics, Volume 63, 1999, pp. 347-374.

17. Seshadri, B. R. and Newman, J. C., Jr., "Analyses of Buckling and Stable Tearing in Thin-Sheet Materials," ASTM STP 1332, 1999, pp. 114-134. (Also NASA TM 208428, May 1998)

18. Seshadri, B. S., Newman, J. C., Jr., Dawicke, D. S. and Young, R. D., "Fracture Analysis of the FAA/NASA Wide Stiffened Panels," NASA TM 208976, December 1998. (Also in NASA CP 208982, Part 2, 1999, pp. 513-524)

19. Young, R. D., Rouse, M., Ambur, D. R. and Starnes, J. H., Jr., "Residual Strength Pressure Tests and Nonlinear Analyses of Stringer- and Frame-Stiffened Aluminum Fuselage Panels with Longitudinal Cracks," NASA CP 208982, Part 2, pp. 408-426.

20. Luxmoore, A., Light, M. F. and Evans, W. T., "A Comparison of Energy Release Rates, the J-Integral and Crack Tip Displacements," International of Journal of Fracture, Vol. 13, 1977, pp. 257-259.

21. Paleebut, S., "CTOD and COD Measurements on Compact Tension Specimens of Different Thicknesses," M.S. thesis, Michigan State University, East Lansing, Mich., 1978.

22. Schwalbe, K. -H. and Hellmann, D., "Correlation of Stable Crack Growth with the J-Integral and the Crack Tip Opening Displacement," GKSS Report 84/E/37, 1984.

23. Reuter, W. G., Graham, S. M., Lloyd, W. R. and Williamson, R. L., "Ability of Using Experimental Measurements of w to Predict Crack Initiation for Structural Components," ESIS Pub. 9, 1991, pp. 175-188.

24. Lloyd, W.R., and Piascik, R.S., "Three Dimensional Crack Growth Assessment by Microtopographic Examination," Fracture Mechanics 26th Volume, ASTM STP 1256, Walter G. Reuter, John H. Underwood and James C. Newman, Jr., Eds., American Society for Testing and Materials, Philadelphia, 1995.

25. Newman, J. C., Jr., Bigelow, C. A. and Dawicke, D. S., "Finite-Element Analyses and Fracture Simulation in Thin-Sheet Aluminum Alloy," Durability of Metal Aircraft Structures, Proceedings International Workshop on Structural Integrity of Aging Airplanes, S.N. Atluri, C.E. Harris, A. Hoggard, N. Miller and S.G. Sampath, eds., W.H. Wolfe Associates, Alpharetta, Georgia, 1992. (Also in NASA TM 107662, August 1992)

26. Dawicke, D. S. and Sutton, M. A., "Crack Tip Opening Angle Measurements and Crack Tunneling under Stable Tearing in Thin Sheet 2024-T3 Aluminum Alloy," NASA CR 191523, September 1993.

27. Mahmoud, S.H., Ph.D. Dissertation, "Thickness Effects On The Critical Crack Tip Opening Angle Fracture Criterion In 2024-T351 Aluminum", Kansas State University, May, 2000.

28. Mahmoud, S.H., Lease, K.B., "The effect of specimen thickness on the experimental characterization of critical crack-tip-opening angle in 2024-T351 aluminum alloy," Engineering Fracture Mechanics, 2003; 70, 443-456.

29. Sutton, M.A., Chao, Y-J., Lyons, J. S., "Computer Vision Methods for Surface Deformation Measurements in Fracture Mechanics," Novel Experimental Techniques in Fracture Mechanics, ASME VOL. 176, 1993, pp. 203-217.

30. McNeill, S.R., Peters, W.H., Sutton, M.A., "Estimation Of Stress Intensity Factor By Digital Image Correlation," Engineering Fracture Mechanics, 1982; 28(1), 101-112.

31. Burton, W., Mahmoud, S., and Lease, K., "The Effect of Measurement Distance on the Experimental Characterization of Stable Tearing Behavior in Metallic Materials," Journal of Experimental Mechanics, 2004; 44(4), 425-432.

32. Burton W, Frink, E., Mahmoud S, Lease K; unpublished work.

33. Lloyd, W.R., and Piascik, R.S., "Three-Dimensional Crack Growth Assessment by Microtopographic Examination," Fracture Mechanics Vol. 26th ASTM STP 1256, ASTM, Philadelphia, 1995, pp. 303-318.

34. Sakhalkar, A., Frink, E., Mahmoud, S., Lease, K., "CTOA Measurement Methods and Crack Tunneling in 2024-T351 Aluminum Alloy," Strain: An International Journal for Experimental Mechanics, 2008; published online, DOI: 10.1111/j.1475-1305.2008.00579.x. Volume 47, Issue s1, June 2011, Pages: e130–e141.

35. Heerens, J., Schodel, M., "On the determination of crack tip opening angle, CTOA, using light microscopy and δ_5 measurement technique," Engineering Fracture Mechanics, 2003; 70, 417-426.

36. Schwalbe, K.-H., Newman, J. C., Jr., Shannon, J. L., Jr., "Fracture mechanics testing on specimens with low constraint – standardization activities within ISO and ASTM," Engineering Fracture Mechanics, 2005; 72, 557-576.

37. Darcis, Ph.P., McCowan, C.N., Windhoff, H., McColskey, J.D., Siewert, T.A., "Crack tip opening angle optical measurement methods in five pipeline steels," Engineering Fracture Mechanics, 2008; 75, 2453-2468.

38. Darcis, Ph.P., McColskey, J.D., McCowan, C.N., Siewert, T.A., "Exploring Methods for Measuring Pipe Weld Toughness," Welding Journal, 2007; 86(6), 48-50.

39. Ph.P Darcis, C.N. McCowan, E.S. Drexler, J.D. McColskey, A. Shtechman, T.A. Siewert, "Fracture Toughness Through a Welded Pipeline Section – Crack tip opening criterion," Welding in the World, 2007; 51(Special Issue), 225-234.

40. Frink, E. and Lease, K., "Characterization of Stable Tearing in Various Metallic Alloys using the CTOA and δ_5 COD Fracture Parameters," 12th International Conference on Fracture Proceedings, 2009; Ottawa, Canada.

41. Dawicke, D.S. and Sutton, M.A., "CTOA and Crack Tunneling Measurements in Thin Sheet 2024-T3 Aluminum Alloy," Experimental Mechanics, 1994; 34(4), 357-368.

42. James, M.A. and Newman, J.C. Jr., "The Effect of Crack Tunneling on Crack Growth: Experiments and CTOA Analyses," Engineering Fracture Mechanics, 2003; 70(3-4), 457-468.

43. Sutton, M.A., Dawicke, D.S. and Newman, J.C. Jr., "Orientation Effects on the Measurement and Analysis of Critical CTOA in an Aluminum Alloy Sheet," 1995; Fracture Mechanics: 26th Volume, ASTM STP 1256, Walter G Reuter, John H Underwood, and James C Newman Jr., Eds, American Society for Testing and Materials, Philadelphia.

44. James, M.A. and Newman, J.C. Jr., "Characterization of Crack Length Measurement Methods for Flat Fracture with Tunneling," Journal of ASTM International, 2005; 2(3), 31-46.

45. Shivakumar, K.N., and Newman, J.C. Jr., "ZIP3D – An Elastic-Plastic Finite Element Analysis Program for Cracked Bodies," NASA Technical Memorandum 102753, November 1990.

46. Lan, W., Deng, X., and Sutton, M.A., "Investigation of crack tunneling in ductile materials," Engineering Fracture Mechanics, 2010; 77, 2800-2812.

47. Newman, J.C. Jr., and Lease, K., "Fracture under Low-Constrain Conditions – from Laboratory Coupons to Structural Applications," Plenary Lecture; 12th International Conference on Fracture Proceedings, 2009; Ottawa, Canada.

48. James, M.A. and Johnston, W.M., "A Relationship Between Constraint and the Critical Crack Tip Opening Angle," 11th International Conference on Fracture Proceedings, 2005; Turin, Italy.

49. Mahmoud, S. and Lease, K., "Two-dimensional and three-dimensional finite element analysis of critical crack-tip-opening angle in 2024-T351 aluminum alloy at four thicknesses," Engineering Fracture Mechanics, 2004; 71, 1379-1391.

Chapter 2 – CTOA Measurement Methods and Crack Tunneling in 2024-T351 Aluminum Alloy

By Aditya Sakhalkar, Elizabeth Frink, Samer Mahmoud, Kevin Lease

*Published online in "Strain: An International Journal for Experimental Mechanics", 30 Dec 2008, DOI : 10.1111/j.1475-1305.2008.00579.x; then published in Volume 47, Issue s1, June 2011, Pages: e130–e141

**Note: Experimental and computational work performed by Sakhalkar, Mahmoud and Lease; analysis and writing completed by Frink and Lease

View article at: http://onlinelibrary.wiley.com/doi/10.1111/j.1475-1305.2008.00579.x/abstract

Chapter 3 – Multiple-Method CTOA Stable Tearing Characterization of Three Metallic Alloys

By Elizabeth Frink and Kevin Lease

*Accepted for "Journal of Testing and Evaluation", April 2012 – this is the pre-publication manuscript

**Note: Experimental work performed by Sakhalkar, Mahmoud and Lease; analysis and writing completed by Frink and Lease

Over the past several years the crack tip opening angle (CTOA) has been identified as one of the most promising fracture parameters to characterize low constraint stable tearing and instability in structural metallic alloys. This study presents the results of experimental stable tearing characterizations performed on three typical structural metallic alloys – two aerospace grade aluminums and a titanium alloy. Specific attention is given to the measurement methods used, and the correlation between CTOA and Delta-5. The effect of material and measurement method on CTOA is observed and a clear relationship is seen.

Keywords: crack tip opening angle, crack opening displacement, delta-5, stable tearing

Introduction

The general failure process for a metallic material that undergoes large amounts of plastic deformation near a pre-existing sharp crack in low constraint conditions has been shown to consist of three distinct stages: (1) crack blunting/initiation, (2) stable crack extension, and (3) unstable crack extension after maximum load carrying capacity is reached. The crack tip opening angle (CTOA) fracture parameter has shown promise in characterizing and predicting stable crack growth and instability [1-9]. In general, the CTOA parameter can be thought of as the angle made by the crack flanks emanating from the crack tip (as illustrated in Figure 3.1-(a)), however, the basis of this paper is to evaluate three specific analytical methods used to define this parameter from actual stable tearing test data. The CTOA vs. crack extension (Δa) behavior during stable tearing tests on laboratory specimens has been shown by several researchers to start out with a relatively high angle and abruptly drop to a relatively constant angle. This constant "plateau" is often referred to as the "critical" crack tip opening angle and the high angle region has been shown to be associated with significant tunneling. An example of this CTOA-Δa behavior is shown in Figure 3.1-(b) for sheet 2024-T351 Al.

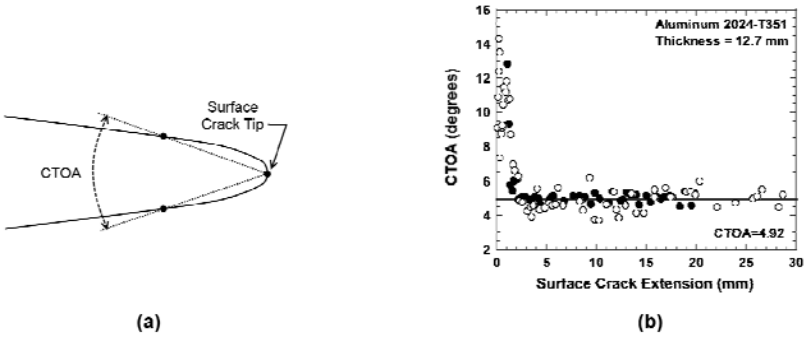

Figure 3.1: Overview of CTOA parameter: (a) illustration of how CTOA is defined, and (b) example CTOA data showing initial high region dropping to lower, constant region

The primary goal of this study was to investigate three methods of measuring the CTOA parameter from experimental stable tearing test results. The secondary goal of the current study was to investigate the CTOA values obtained from the δ_5-resistance curves and compare these values to the results of the three CTOA measurement methods.

CTOA Measurement Methods

The three methods employed in this study use at least one of three "ranges" which are shown in Figure 3.2. The more specific locations and uses of these ranges used in each method will be discussed in the upcoming subsections. However, in general the "surface crack tip" is the visible point on the surface where the crack flanks come together and hinge. The "reference range" is a small range which is not far behind the surface crack tip while the "baseline range" extends longer and is further behind the surface crack tip. This terminology is used throughout. Each method uses sets of points along the crack flanks to define the CTOA for each stable tearing event. The procedure used to select these points and use them to calculate CTOA is unique to each method.

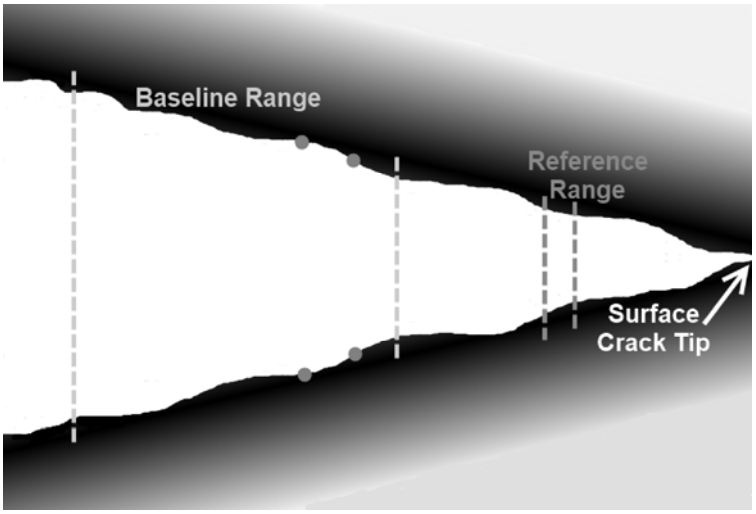

Figure 3.2: Illustration of the three general "ranges" used in the three measurement methods

As a crack tip advances from the local fatigue pre-crack region, the CTOA value follows a given trend which is influenced by the method of measuring CTOA. In optical microscopy (OM) measurement of CTOA (as used in this study), user-defined measurement ranges follow along on the crack flanks as the crack tip progresses, and in the early stages of crack propagation the crack flanks experience several phases in general shape/separation. Due to these phases and inherent differences in measurement methods, when methods determine CTOA in different ways within the same measurement ranges, it can be expected that they may produce different values/trends in CTOA. The phases that the crack flanks experience are listed below and are illustrated in

Figure 3.3. The two phases shown in italics may not be observed in all materials and do not deal with the shape of the flanks, so they are not included in the figure.

A. Reference range enters the initial crack region

B. Baseline range enters the initial crack region

C. Baseline range exits the blunting region (region prior to the pre-crack tip)

D. Tunneling extent remains constant

E. Flat to slant transition complete

The general behaviors of the different methods are driven by these phases and they reveal the differences in geometries of the flanks in the initial advancing of the crack tip. Idealized behaviors and curves of each method are discussed below using Figure 3.4 (based on what must happen due to the nature of the measurement method), with relation to each of the observed phases in the crack flank shapes.

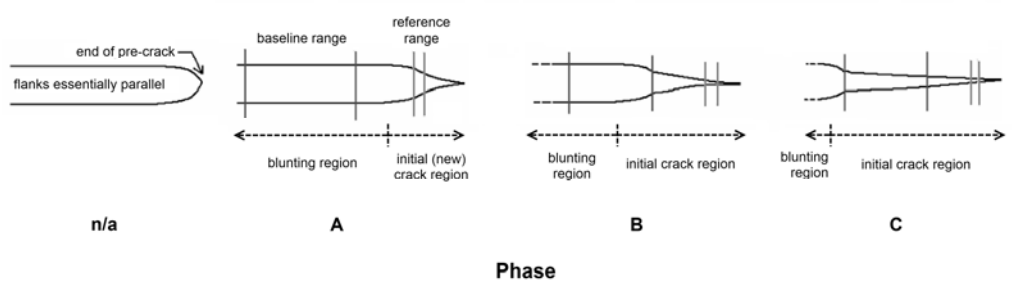

Figure 3.3: Illustration of the defined phases that the crack flanks experience as the measurement ranges follow the progressing surface crack tip

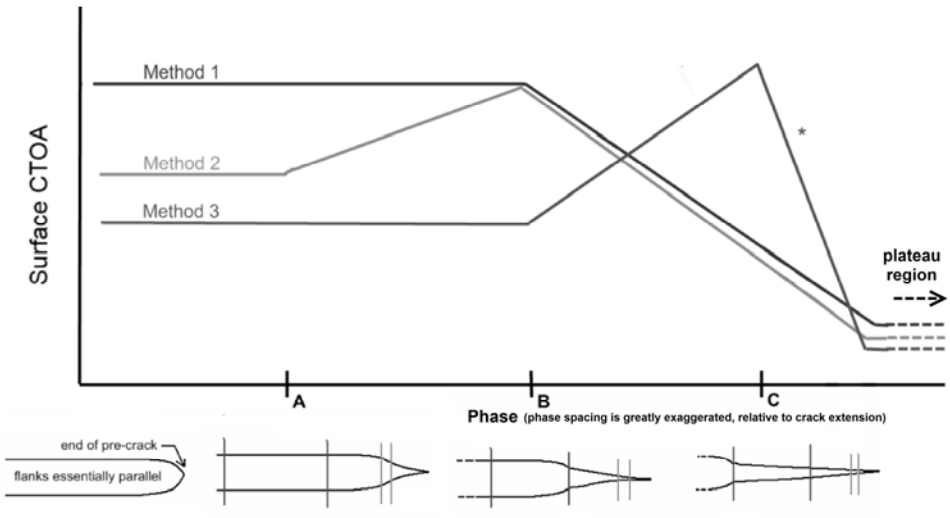

Figure 3.4: Idealized trends for each method in the initial non-constant CTOA region (only the first several mm of surface crack extension). The x-axis is essentially the amount of surface crack extension, but is not to scale because the phases are shown instead

CTOA Measurement Method 1

Following the guidelines provided by ASTM E2472-06 [10] closely, Method 1 measures CTOA at each tearing event by extending lines from the crack tip to matching sets of points on the top and bottom flanks, as shown in Figure 3.5-(a). Nine measurements are made at set intervals (0.125 mm) in the baseline range and the average of these measurements is the Method 1 CTOA for a single tearing event. This method is the only method in the current study that uses the crack tip in the CTOA measurement, is generally considered the "traditional" experimental method for determining CTOA and has been used and discussed by Dawicke and Sutton [1], Burton et al [5], Schwalbe et al [6], Darcis et al [8] and Sakhalkar et al [9], among others.

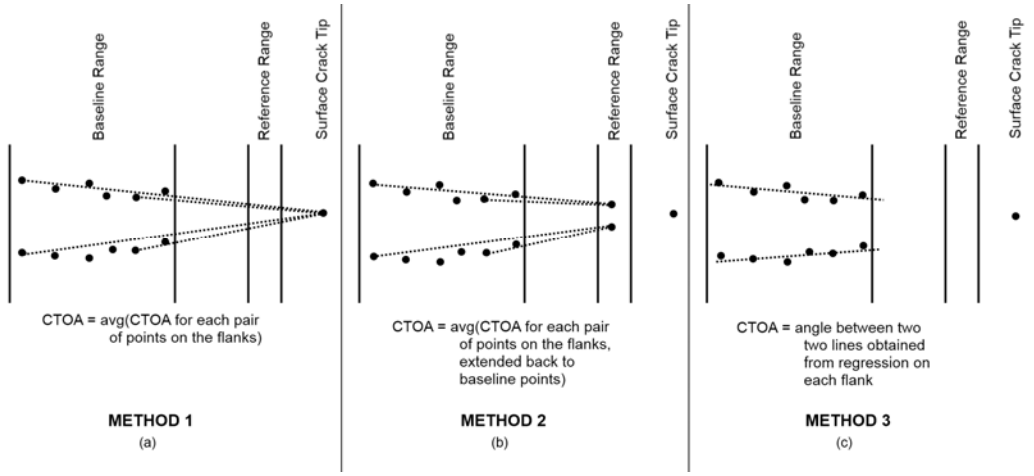

Figure 3.5: General illustration of the selection of points in the three "ranges" and how the CTOA is defined using the points, for (a) Method 1, (b) Method 2, and (c) Method 3

Generally speaking, the CTOA values obtained from Method 1 start high and then decrease to a nearly constant value (idealized curve shown in Figure 3.4). Method 1 does not include the reference range, so Phase A does not affect the CTOA values. Due to the nature of Method 1, as the baseline range enters the initial crack region at Phase B, the CTOA values begin to decrease and continue decreasing through Phase C. This is due to the crack flanks being closer together in the initial crack region (see the generalized sketch of these phases for Method 1 in Figure 3), and as more of the nine individual CTOA values are taken in the initial crack region, the average CTOA value decreases. Shortly after beginning Phase C, the CTOA values level out to a constant value. This same behavior around Phase C was observed by Burton, et al [5].

CTOA Measurement Method 2

An alternative method has recently been introduced that uses only the crack flanks to determine the CTOA values [3, 6, 8-9, 11-12]. Rather than use the crack tip, a pair of points on the crack flanks within the reference range are used in the measurement and the angle is calculated based on distances between the flanks. Method 2 in the current study is a variation of this method (see Figure 3.5-(b)). In the current study, the pair of points in the reference range is set (for consistency) at 0.15 mm behind the crack tip. Four measurements are made in the baseline range (0.5 to 1.5 mm behind the crack tip at 0.333 mm intervals). The individual CTOA at a measurement location in the baseline range is given by:

$$CTOA_i = \frac{\delta_i - \delta_0}{r_i} \qquad (3.1)$$

where δ_0 is the displacement of the flanks at the reference point in the reference range, δ_i is the displacement of the flanks at measurement location i in the baseline range and r_i is the distance from that measurement location to the reference point. For more details on this method, see reference [9]. An important note on this method is that the vertex of the angle defined by the extended flanks is not forced to meet the surface crack tip. If the vertex of the measurement angle is located, it may converge at a point behind or beyond the actual crack tip. Potential applications to crack front tunneling prediction will be briefly described at the end of the next section.

As seen in Figure 3.4, the idealized curve (representing the nature of the method) for Method 2 begins at a high value as Method 1 did, but begins lower than the initial value for Method 1. When Phase A occurs, the CTOA values for Method 2 increase sharply because this is where the difference between the displacement in the baseline range and the reference range increases sharply (see the generalized sketch for Phase A in Figures 3.3 and 3.4). Since the CTOA values for Method 2 are calculated based on that difference, the CTOA values increase with the increase in the difference. When Phase B occurs, the measured CTOA values begin to decrease and continue decreasing through Phase C. The decrease at Phase B occurs because the baseline range begins to enter the initial crack region where the flanks are closer together (a generalized sketch of this phase is shown in Figure 3.3), so the displacements in the baseline range will begin to decrease while the displacement at the reference range stays approximately the same as it was prior to Phase B. Since the vertex of the extended lines is not forced to lie at the surface crack tip and may actually extend beyond it, a slightly lower constant CTOA value than Method 1 may be obtained entering into Phase C.

CTOA Measurement Method 3

An additional alternative method recently introduced [8, 9] defines sets of points in the baseline range only and uses linear regression to fit a line to these points for each flank. The angle between these two lines is then used to determine CTOA, as seen in Figure 3.5-(c). More details on this method (referred to as Method 3 in this study) can be found in reference [9]. Similar to Method 2, this method also does not force the defined lines to intersect the surface crack tip. If the defined lines are extended to their vertex, it may lie behind or beyond the actual crack tip.

Similar to Methods 1 and 2, the idealized curve (Figure 3.4) for Method 3 also starts at a high CTOA value, but begins at a value lower than the initial value for both Methods 1 and 2. Measurements in the reference range are also not included in Method 3, so Phase A does not have an effect on the CTOA values of this method. At Phase B, a sharp increase in CTOA values is observed. This is because the tip of the regression lines closest to the crack tip are drawn closer together as the baseline range enters the closer together flanks in the initial crack region (Figure 3 shows the generalized sketch of this phase), which makes a larger angle between the lines. As the baseline range exits the blunting region completely in Phase C, the ends of the regression lines furthest from the crack tip are also drawn together. This makes the lines more parallel and causes a decrease in the measured CTOA values (unless the flanks are already quite parallel before reaching this phase.

As a side note, recall that in Methods 2 and 3 it is possible for the vertex of the angle to converge beyond the surface crack tip. Although not the focus of this study, it is of interest to determine if the "projected crack tip" from these methods correspond to a potentially internally tunneled crack tip. This interest was investigated on the 2024-T351 Al as it was tested with fatigue marker bands applied so the location of the crack tip was known [9]. However, in this study, it was found that there was no correlation between the projected crack tip and the tunneled crack tip.

Experimental CTOA Results

Three different alloys were selected for this study – 2024-T351 aluminum (Al) (thickness B = 6.35 mm), 5083-H321 Al (B = 3 mm) and Ti-6Al-4V titanium (B = 1.35 mm). Standard compact tension (C(T)) specimens (W = 152 mm) were fabricated in the L-T orientation from these materials. Fatigue pre-cracking (R = 0.1) was performed to an initial crack-to-width ratio of $a_0/W = 0.4$ at load levels to ensure that the ratio of stress intensity factor range to Young's Modulus ($\Delta K/E$) would be below 0.005 $\sqrt{mm}$. Stable tearing fracture tests were then performed, using anti-buckling guide plates, at a constant displacement rate of 0.002 mm/sec. Several stages of crack growth were observed in each test, where the initially sharp pre-crack tip blunted until a tearing crack initiated and propagated. For each fracture test, an OM setup (see reference [1] for more detail) enabled post-test measurement of CTOA, Δa and δ_5 values, where Δa is the surface crack extension measured from the end of the pre-crack. Four specimens from the 2024-T351 Al were tested and three specimens each of the 5083-H321 Al and the Ti 6-4 were tested.

Material Behavior

The three selected materials exhibited distinct stable tearing behaviors in this study. Fracture type and initial flank shapes were the main aspect that varied between materials. For 2024-T351 Al, the flanks remained in flat fracture for the entirety of the test. On the other hand, the Ti 6Al-4V (Ti 6-4) transitioned to pure slant fracture before fatigue pre-cracking was complete, and remained in slant fracture for the entirety of the test (through the critical CTOA surface crack extension range – this range is discussed in more detail in a later section). Behaving between the two extremes, a transition from flat to slant fracture was observed in the 5083-H321 Al after a short amount of stable crack extension (Δa approximately equal to that of the thickness of the specimens). Due to the flat fracture observed in the 2024-T351 Al, meandering and jagged crack flanks (as seen in Figure 6) were the characteristic flank type for this material. Exhibiting slant fracture during most, if not all, of the stable crack extension, both the 5083-H321 Al and the Ti 6-4 had much smoother and straighter flanks (Figure 3.6).

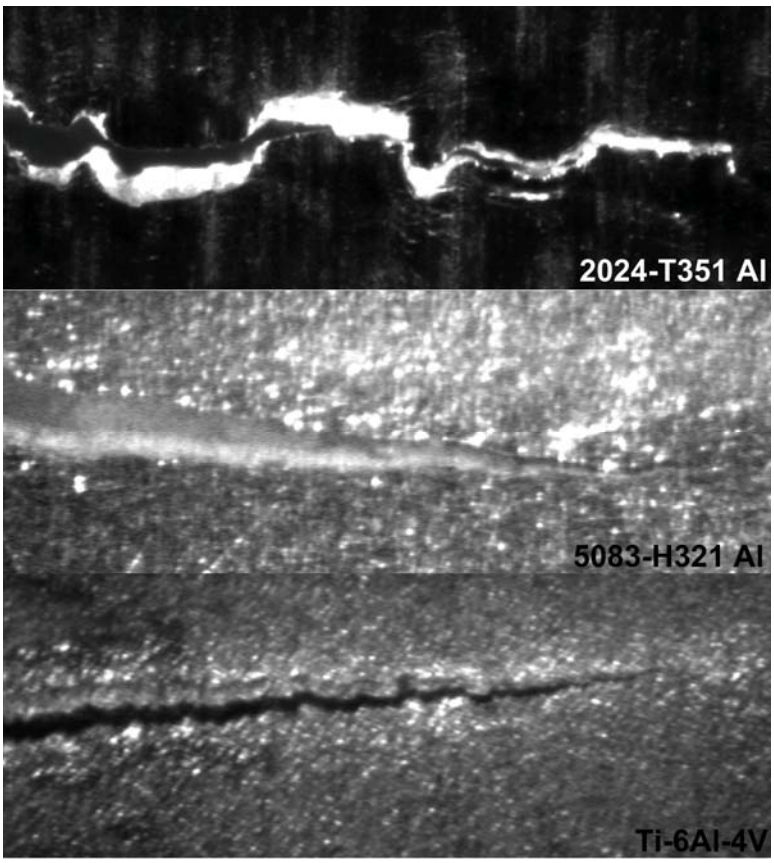

Figure 3.6: Flank shapes, due to fracture type, for the three materials in this study

Close inspection of the advancing crack in the region near to the pre-crack tip reveal distinct differences in crack flank shapes shown in Figure 3.7. The crack progresses from the pre-crack tip in a tapered, blending transition in the 5083-H321 Al, while in the Ti 6-4 the stable tearing crack is a distinct crack from the pre-crack, with closer, more parallel flanks. The 2024-T351 Al flank shape falls in between these two distinctly different materials. Burton, et al [5] has observed this same difference in flank shape between the Ti 6-4 and the 5083-H321 Al and has attributed this to the difference in "pinching" (gross plastic deformation) between materials due to differences in tunneling. These differences in flank shape, along with the method behaviors to be discussed, lend explanation to differences in the CTOA-Δa behavior.

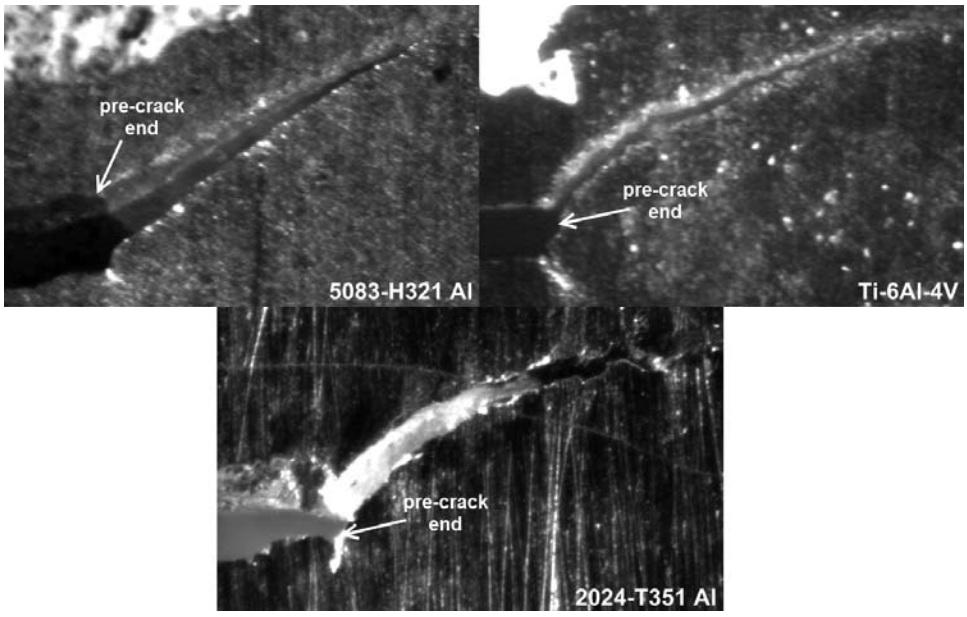

Figure 3.7: Transitions from blunting pre-crack tip region to stable tearing crack region for all three materials in this study

Material and Method Effect on Initial CTOA-Δa Behavior

Combining the effects of differences in materials and the effects of differences in CTOA measurement methods, different trends can be observed in the initial portion of each CTOA-Δa curve. Figures 3.8-3.10 show the initial portions of the CTOA-Δa plots for each material, where each data point represents a single stable tearing event. The phases A-D are shown below the x-axis in parentheses. Please note that each stable tearing test exhibited approximately 20-25 mm of overall crack extension with only the initial 6 mm shown here to focus on the trends in the initial stable tearing region. The trend lines were drawn by hand, and as only the first 6 mm of

crack extension is shown, the constant region of CTOA does not represent the exact critical CTOA for the set of data.

2024-T351 Aluminum Alloy

In the 2024-T351 Al, Method 1 CTOA values exhibited the typical CTOA-Δa trend, which was illustrated earlier in Figure 3.1-(b), with only a slight initial increase in CTOA prior to the peak. However, for Method 2 CTOA increased sharply from a lower initial value to a maximum (with a barely noticeable dip in the peak) and then sharply decreased to a constant value. Method 3 also exhibited an atypical trend, starting at an even lower initial value than Method 2, with a sharp, but more gradual increase to a maximum then a sharp decrease to a fairly constant CTOA value. This initial non-constant CTOA region for the 2024-T351 Al is shown in Figure 3.8, with the measurement method phases indicated.

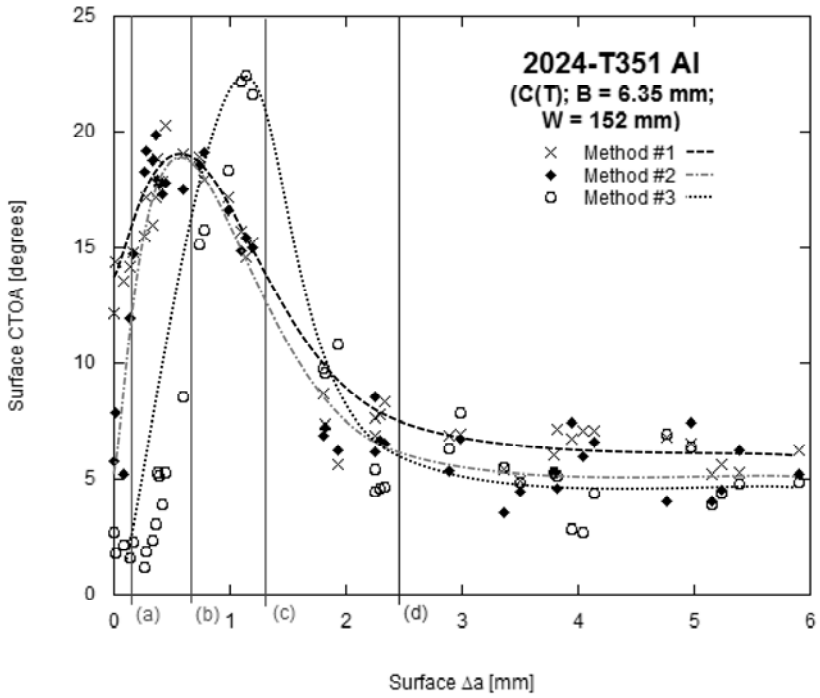

Figure 3.8: Initial non-constant CTOA region for 2024-T351, with vertical lines indicating where each phase occurs

5083-H321 Aluminum Alloy

Figure 3.9 shows the initial non-constant CTOA region for 5083-H321 Al. CTOA values for 5083-H321 Al obtained by Method 1 and Method 2 increased sharply from an initially low value to a maximum and then sharply decreased to a constant value. Method 3 exhibited a sharp, but slower increase from a very low value to a maximum with a sharp decrease to a constant value.

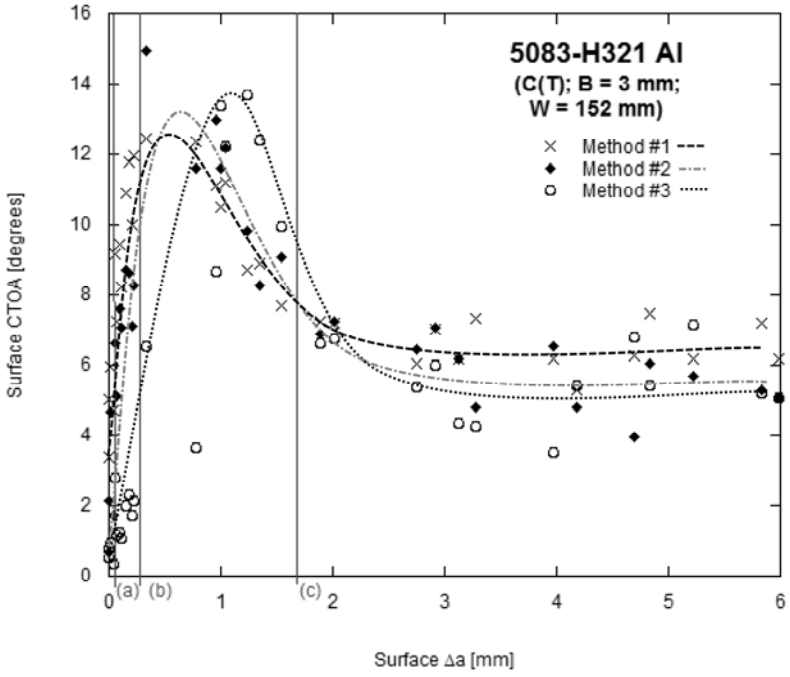

Figure 3.9: Initial non-constant CTOA region for 5083-H321 Al, with vertical lines indicating where each phase occurs

Ti-6Al-4V Titanium Alloy

The trends observed in Ti 6-4 were the most atypical of the trends in the current study. Method 1 started at a maximum (with only a slight initial increase) and then sharply decreased to a constant value. Method 2 started low and sharply increased to a maximum and then sharply decreased to a constant value. Method 3 started low and sharply increased to a small peak, valley and then a constant value. Method 2 was the only method in this material that exhibited the typical decrease from a maximum to the constant value. These trends for Ti 6-4 can be observed in Figure 3.10 and can most likely be explained by the fact that the Ti 6-4 was transitioned to slant fracture before pre-cracking finished, if in fact the initial high CTOA values in a typical CTOA-Δa curve are due to significant tunneling. In slant fracture little to no tunneling occurs so it is expected that

there would be minimal initial high CTOA values if no tunneling occurs, which is what was observed in the Ti 6-4.

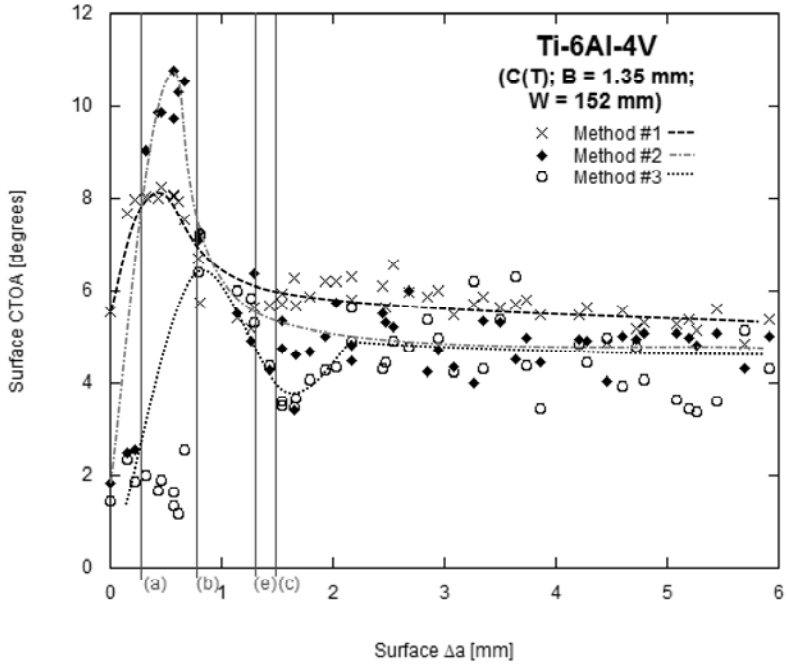

Figure 3.10: Initial non-constant CTOA region for Ti-6Al-4V, with vertical lines indicating where each phase occurs

Experimental Critical CTOA

Taking into consideration the material and the CTOA measurement method, an interplaying relationship can be observed on the entire CTOA-Δa curves (not limited to the initial 6 mm). It is quite clear that the material has a strong role in the critical CTOA during stable tearing. However, there is also some "interference" from the CTOA measurement method. Figures 3.11-3.13 present the overall CTOA-Δa behavior for Method 1-3, respectively, with all three materials in each. From the results represented in these figures, the constant value (plateau) that each CTOA-Δa curve eventually achieves is defined as the critical experimental CTOA value, Ψ_{ce}. The critical value was obtained from the experimental CTOA versus crack extension data by averaging the CTOA values (for a given measurement method) in the range $\Delta a_{min} < \Delta a < \Delta a_{max}$, where Equations 3.2 and 3.3 define Δa_{min} and Δa_{max} [10].

$$\Delta a_{\min} = 50/(5+B) \tag{3.2}$$

$$\Delta a_{\max} = W - a_0 - 4B \tag{3.3}$$

Comparisons of the critical experimental CTOA values obtained for each material and each method are shown in Table 3.1. The coefficients of variation (COV, ratio of standard deviation to average value) for each material and method are also included in Table 3.1. Regardless of material, measurement Method 1 produced the highest critical experimental CTOA and the lowest COV. This may be due to a variety of reasons, including the fact that this method uses the actual crack tip but does not use the reference range (which is very near the crack tip and can induce scatter [5]).

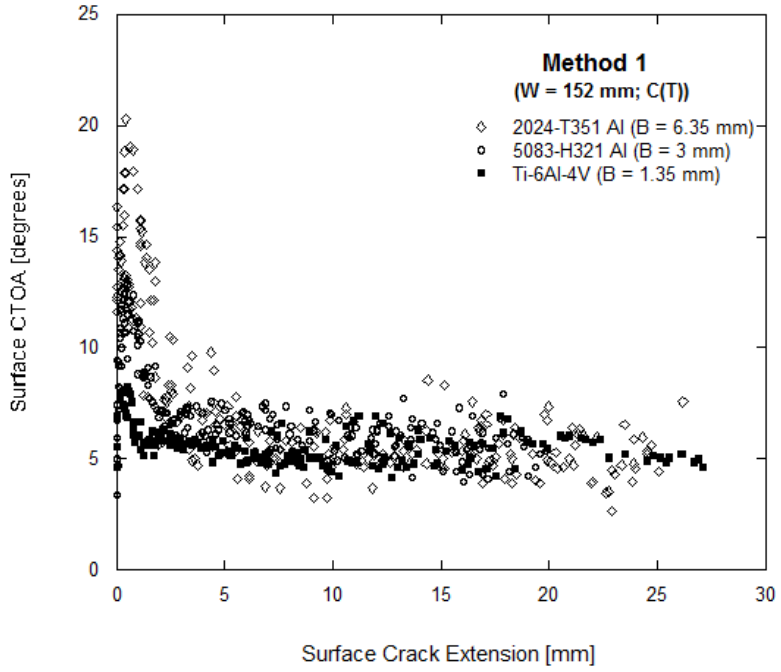

Figure 3.11: Method 1 CTOA measurements for all materials in the current study [13]

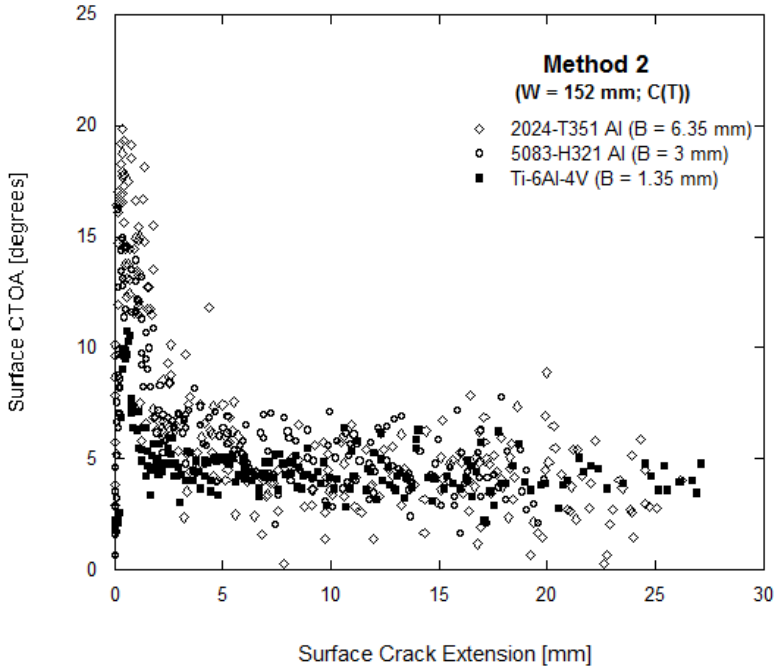

Figure 3.12: Method 2 CTOA measurements for all materials in the current study [13]

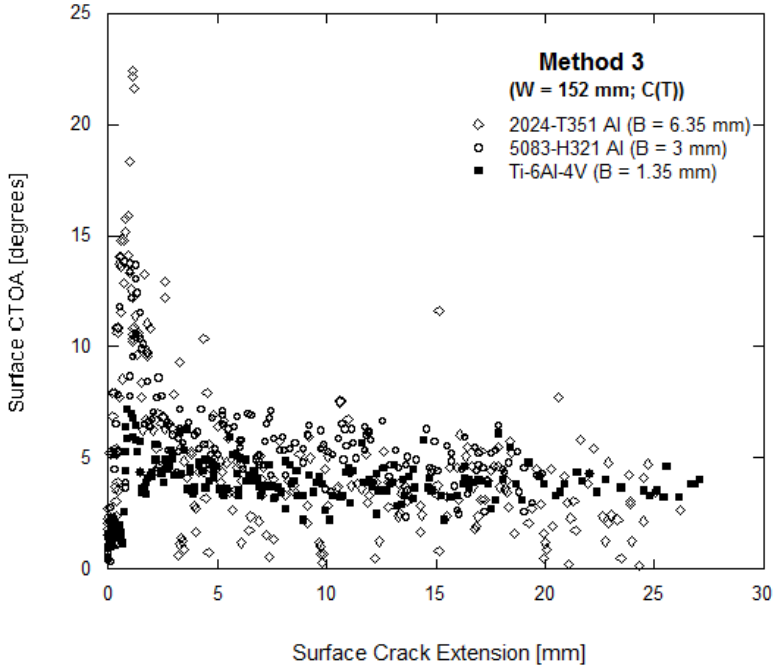

Figure 3.13: Method 3 CTOA measurements for all materials in the current study [13]

Table 3.1: Comparison of experimental critical CTOA values obtained in the current study for multiple measurement methods and multiple materials [13]

	Critical CTOA (Ψ_{ce})					
	2024-T351 Al (4 tests, B=6.25mm)		5083-H321 Al (3 tests, B=3mm))		Ti-6Al-4V (2 tests, B=1.35mm)	
	Average [deg]	Coeff. of Variation	Average [deg]	Coeff. of Variation	Average [deg]	Coeff. of Variation
Method 1	5.48	0.20	5.93	0.15	5.37	0.13
Method 2	4.26	0.38	4.71	0.28	4.28	0.19
Method 3	3.64	0.50	5.04	0.22	3.81	0.19
δ_5-Δa	3.62	--	5.55	--	2.52	--

Looking strictly at the material dependency of the COV, the 2024-T351 Al exhibited the highest COV across the methods while the Ti 6-4 exhibited the lowest. This trend was rather pronounced for these two materials for Methods 2 and 3 at a factor twice or more. This is likely explained by the jagged crack flanks observed for the 2024-T351 Al (resulting in larger scatter in measurements) and the smooth, parallel flanks observed in the Ti 6-4 (resulting in less scatter).

Regardless of the measurement method, the 5083-H321 Al alloy had the largest critical CTOA. The smallest critical CTOA value depended on which method was employed. Looking only at the three CTOA measurement methods (Method 1, 2 and 3), the largest CTOA (independent of the material) was obtained using Method 1 and the smallest CTOA depended on the material. This may be partially explained by a trend observed by Burton, et al [5] – closer than 0.5 mm to the crack tip, the single-point CTOA measurement non-linearly increases and the measurement decreases. Thus, Method 2, which incorporates the reference range (which is closer than 0.5 mm), is forced to include points on the flanks that are on a steeper slope than the further part of the flank.

Combining material and method, Method 3 measurements in the 2024-T351 Al resulted in the largest amount of scatter of the three materials and of the three methods. Method 3 relied solely upon the crack flank shapes in the baseline range. As the 2024-T351 Al exhibited flat fracture (led to jagged crack flanks), this may explain the large COV.

Measurement of δ_5

The δ_5 parameter tracks the vertical displacement between two corresponding points that are originally 2.5 mm above and below the pre-crack tip before any stable crack extension has occurred. This was originally developed by Hellmann and Schwalbe [14-15]. Using a speckle coating, δ_5 was measured with a pattern matching technique for every stable tearing event.

Experimental δ_5 Results

Experimental δ_5 results define a fracture resistance curve for the given material and specimen. As will be discussed in this section, these results can then be used to derive CTOA results as well. This provides another comparison to the measurements obtained thus far in previous sections.

Overall δ_5 R-curve Behavior

Figure 3.14 shows the δ_5 R-curve for each material in the current study. All results from the series of tests for a given material were combined to produce one R-curve for the material. In C(T) specimens, it has been suggested [3, 10] that the δ_5 parameter is geometry independent and coincides with optically measured CTOA data well within the range in Equation 3.4,

$$\Delta a < 0.25(W - a_0), \qquad (3.4)$$

so any δ_5 measurements beyond this limit were not included in the data sets. As can be seen in Figure 14, the individual specimen curves for the two aluminum alloys were within a relatively small scatter band. The early behavior of the δ_5 R-curve for the two aluminum alloys was very similar and then they began to deviate from one another around 10 mm of surface crack extension with the 5083-H321 Al displaying the higher fracture resistance. The Ti 6-4 displayed the lowest fracture resistance. This corresponds with the parallel, close flanks observed in the Ti 6-4. In addition, the Ti 6-4 also exhibited the least amount of scatter.

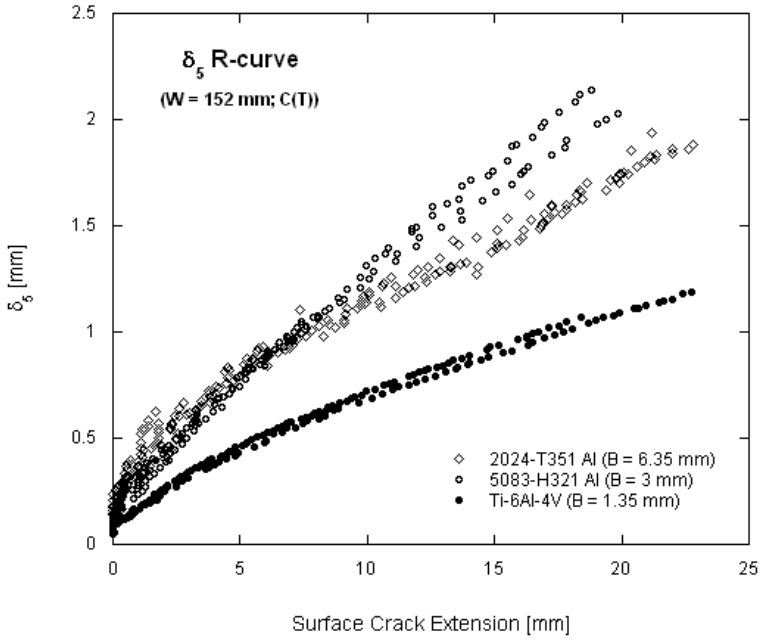

Figure 3.14: R-curves for the δ_5 parameter for each material in this study [13]

CTOA-Δa and Critical CTOA from δ_5 R-curve

A relationship between the δ_5 R-curve and CTOA value has been proposed by Heerens and Schodel [3] and presented in Appendix X2 of [10] – the incremental slope of the δ_5 R-curve may be representative of the incremental CTOA, which can be used to determine a critical CTOA. In order to determine incremental slopes of each δ_5 R-curve in this study, the derivative of exponential fits ($ae^{bx} + ce^{dx}$) were obtained and point-by-point slopes were calculated using the experimentally measured surface crack extension. The resulting CTOA-Δa R-curves from the δ_5 data are shown in Figures 3.15-3.17 (by material), and compared to the optically measured CTOA values from Method 1 ($CTOA_{op}$). As seen in Figure 3.16, the resulting CTOA-Δa R-curves for the 5083-H321 Al fell within the scatter of the optically measured CTOA values (Method 1) for all of the data up to Equation 3.4 from the previous section. Conversely, the Ti 6-4 CTOA-Δa R-curves from δ_5 (Figure 17) fell significantly lower than the optically measured CTOA values from Method 1, but mimicked the trend of the curve. The results for the 2024-T351 Al (Figure 15) fell slightly below the scatter of the optical measurements. Note that only Method 1 was used as an example for comparison, for simplicity purposes.

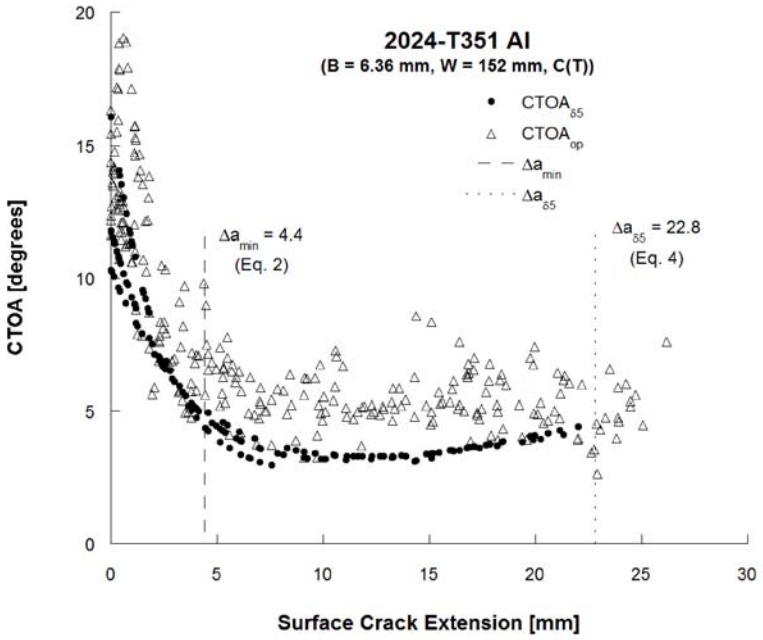

Figure 3.15: CTOA-Δa curve from δ_5 data, compared to Method 1 results, for 2024-T351 Al

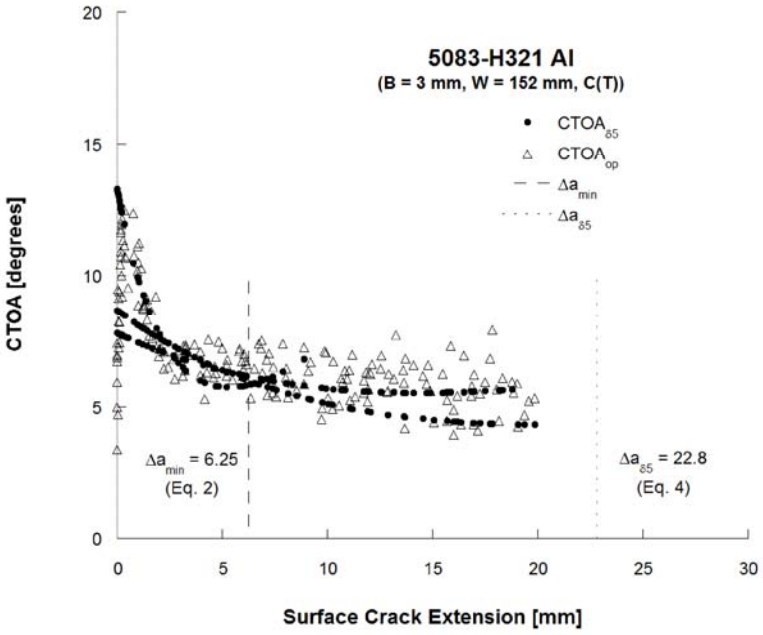

Figure 3.16: CTOA-Δa curve from δ_5 data, compared to Method 1 results, for 5083-H321 Al

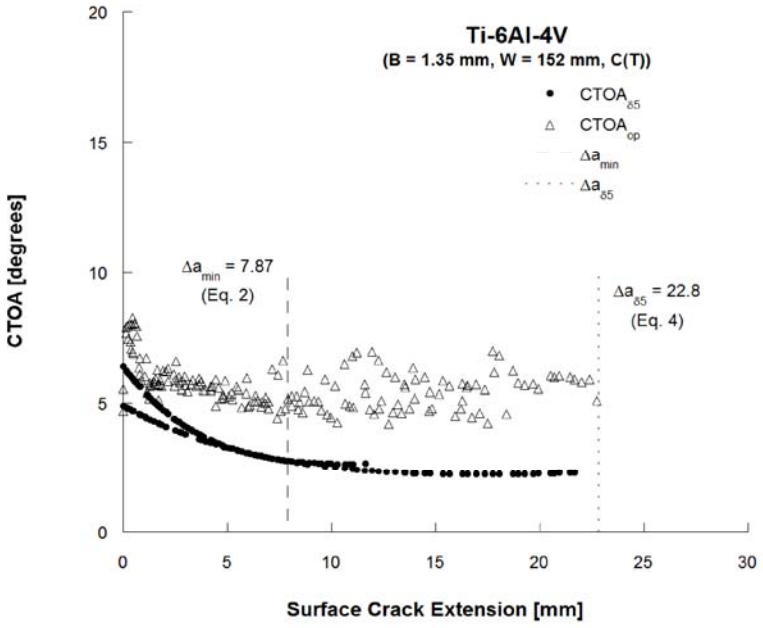

Figure 3.17: CTOA-Δa curve from δ_5 data, compared to Method 1 results, for Ti-6Al-4V

A critical CTOA value was obtained from each CTOA-Δa curve from δ_5 within the minimum crack extension for CTOA provided in Equation 3.2 and the maximum crack extension for δ_5 provided in Equation 3.4. These ranges are shown in Figures 3.15 to 3.17 for each material. The value obtained from Equation 3.4 is independent of specimen thickness or material, and since all three materials had the same W and pre-cracking ratio, the limit obtained from Equation 4 was the same for all three materials. It should be noted that for all three materials, Δa_{max} from Equation 3.3 was significantly beyond the extent of Δa for data collected in this study for all materials. Note that the optically measured CTOA-Δa data extends slightly further than the CTOA-Δa from δ_5. However, this data was also well within the maximum range for Δa as defined in Equation 3. Using the same approach as for CTOA methods, the critical CTOA value was determined by calculating the average value within the mentioned range for Δa for each specimen and then an average was obtained for each material. Table 3.1 includes the average critical δ_5-Δa CTOA values obtained from the series of tests for each material. The correlation between the δ_5-Δa derived critical CTOA and the values obtained from the more direct CTOA measurement methods varies for each material. The δ_5-Δa derived critical CTOA value corresponds closely with the values obtained using the optical methods for the 5083-H321 while

the Ti 6-4 CTOA value from the δ_5 R-curve does not closely correspond to any of the measurement methods. The correspondence between the δ_5-Δa derived CTOA value and the optical measurements in the 2024-T351 Al is somewhat close but there is some disagreement. The significant disagreement in the Ti 6-4 may be attributed to the parallel crack flanks while the slight disagreement in the 2024-T351 Al may be attributed to the observed meandering crack flanks as well as flat fracture/significant tunneling.

It was observed while fitting curves to the δ_5-Δa data and calculating the derivative that the nature of the fit made a significant difference in how well the resulting calculated CTOA-Δa data correlated with the optically measured data. Different fits with an overall goodness of fit resulted in different trends in the CTOA-Δa data from δ_5 which did not correlate well. Some deviated significantly from the optical data before the 22.8 mm limit was reached and some introduced an extra "wave" in the curve after the decrease from the initial high CTOA values. Thus the nature of the fit can have a significant impact on the correlation of the data. This can also cause the upper limit for Δa (Equation 3.4) to include "invalid" data, where the deviation from the optical data has already occurred. In this case, Equation 3.4 would need to be modified to allow less significant crack extension. However, this increases the difference between the ranges for optical CTOA and δ_5 CTOA and it would seem that perhaps Δa_{max} (Equation 3.3) for optical CTOA should be reduced so that it is closer to the limit for δ_5 (Equation 3.4), resulting in better agreement between the δ_5 and optical measurement methods.

Discussion

This paper discussed the results of a purely experimental study that evaluated three direct and one indirect method of determining CTOA from experimental stable tearing data from three materials. In doing so, insight was gained into the initial higher-angle region of the CTOA-Δa curve as well as the constant critical CTOA region. In the initial region, it is widely accepted that the typical high-to-low behavior of the CTOA-Δa curve is associated with significant tunneling. From this study, it has been shown that the measurement technique can also have an impact on this trend, regardless of whether tunneling is present. This is seen in one of the materials investigated in this study (Ti 6-4) which exhibited a transition to slant fracture even during pre-cracking, implying that little or no tunneling was present at the early stages of stable

tearing. Even with little to no tunneling, the Ti 6-4 showed significant differences in the initial behavior of the CTOA-Δa curve, depending on the method employed. Based on the results in Table 3.1 earlier, large scatter exists in the data and there actually appears to be a material dependency on the COV. As discussed earlier, this is expected to be due to differences in crack flank shape (meandering). This may indicate a weakness involved with these types of surface measurement methods if such scatter and inconsistent results are obtained.

In comparing the results of Table 3.1 to other published results, Mahmoud and Lease [16] experimentally characterized critical CTOA for 2024-T351 Al using C(T) specimens (B=6.35, W=203 mm) and determined a value of 5.17 degrees using Method 1 (compared to 5.48 degrees, Table 3.1). Their fracture surfaces exhibited flat-to-slant transition fracture at approximately maximum fracture load during the test. The specimens were surface machined from a 25.4 mm thick plate. It is unclear whether the metallurgical form of the as-received plate and surface machined plate were similar enough for direct comparison. In addition, Heerens and Schodel [3] obtained an experimental critical CTOA value of approximately 5 degrees for 5083-H321 C(T) specimens (B=3 mm), with W=50, 150, and 1000 mm, using a slightly modified Method 1 (compared to 5.93 degrees in this study). In their study, flat-to-slant transition occurred slightly past pre-cracking, as was reported in the current study for 5083-H321 Al. At least some of the discrepancies in critical CTOA could be due to the subjectivity associated with identifying the crack tip during measurement and the normal scatter in the data.

In general, the process of running a stable tearing test (and also collecting crack opening images for each stable tearing event) is very time consuming and ultimately involves dealing with data containing large scatter bands. However, two main advantages may be gained from this: (1) since CTOA is an engineering parameter attempting to explain a material-based phenomenon, it is important to view the stable tearing process in action and (2) computer-based calibrations of CTOA (or CTOA-based predictions) should be able to accurately predict the behavior that is experimentally captured on the surface. Therefore, the interplay between the surface behavior (obtained from studies such as this one) and how it correlates to the computational (interior based) simulations is quite important.

Due to the difficulties, scatter, and objectivity involved with the experimental measurement of CTOA, the most prevalent method over the past few decades to characterize the CTOA

parameter has been a combined experimental/computational "calibration" process (in [2, 4, 7, 9, 17-19], for example). This process involves performing a typical stable tearing test while collecting load-line displacement, load, and crack extension. A three dimensional elastic-plastic finite element-based analysis (using code such as ZIP3D [20]) is then used to iterate on CTOA (or CTOD a distance behind the crack tip) until the computational maximum fracture load closely matches that of the experiment(s). This CTOA is then selected as the critical CTOA (Ψc). It should be noted that these computational CTOA calibrations are based off of a mid-plane (center node) release algorithm. An example relevant to the current study is found in [21] where James, et al used ZIP3D to determine $\Psi c = 6.8$ degrees for 2024-T351 C(T) specimens (B=6.35 mm, W=152 mm). This mid-plane value differs significantly from the experimental surface value for the same material/thickness shown in Table 3.1 of this paper ($\Psi ce = 5.48$ degrees). Mahmoud and Lease [22] found a similar (but less extreme) trend with $\Psi ce = 5.17$ degrees and $\Psi c = 5.6$ degrees using ZIP3D. However, the value $\Psi ce = 5.48$ degrees in Table 3.1 compares favorably with Mahmoud and Lease's ZIP3D value of $\Psi c = 5.6$ degrees. When comparing these experimental versus computational values it must be kept in mind that the experimental values are obtained by averaging what is often a large scatter band, whereas the computational calibration method is essentially a single-point method. In addition, the discrepancies most likely are also due to the differences in constraint between the center of the specimen and the free surface of the specimen (with higher constraint in the center and lower constraint near the surface).

The proposed relationship between δ_5 and CTOA [3] proved to be a reasonable relationship, for the most part, in this study. This may seem the way to go as there is minimal scatter in the δ_5 R-curves and a clip gage or LVDT can be used to measure the displacement, rather than having to post-process a long series of images as in the OM methods. However, this approach is subjective to the type of fit that is selected for use.

With the results shown in this paper and ensuing discussion, it does not appear that any one of the three direct measurement methods has a clear advantage over the others. In the opinion of these authors, Method 1 may provide a very mild preference due to the fact that it is already standardized and it was shown in this study to provide the lowest COV for each material. In

light of the comparison to the computational calibration method, none of the three methods appeared to have an advantage.

Rather that exploring new "methods" of measuring surface CTOA, the more exciting and potentially fruitful approach would be to perform small-scale investigations that would simultaneously probe the state of stress and the 3D shape around the tip of the crack (in situ) during the early and intermediate stages of the stable tearing phenomenon. This can be realized with approaches such as in situ high-energy micro-diffraction/imaging based studies of stable tearing. In this way we can learn more about the stable tearing phenomenon, the interplay between CTOA and constraint, and why the CTOA fracture parameter works as well as it does. This would increase our physical understanding, allow for improved computational verifications, and aid in the development of a constraint based/modified engineering parameter to modify the crack tip opening angle parameter.

Acknowledgments

A portion of this work was supported by the Department of Defense (DoD) through the National Defense Science & Engineering Graduate Fellowship (NDSEG) Program.

References

1. Dawicke, D.S., Sutton, M.A., "CTOA and Crack Tunneling Measurements in Thin Sheet 2024-T3 Aluminum Alloy", Exp Mech 34(4), 1994, pp. 357-368.
2. James, M.A., Newman, J.C. Jr, Johnston, M. Jr, "Three-Dimensional Analyses of Crack-Tip Opening Angles and δ_5-Resistance Curves for 2024-T351 Aluminum Alloy", *Fatigue and Fracture Mechanics: 32nd Volume, ASTM STP 1406*, R.Chona Ed., ASTM International, West Conshohocken, PA, 2002, pp. 279-297.
3. Heerens, J., Schodel, M., "On the Determination of Crack Tip Opening Angle, CTOA, Using Light Microscopy and δ_5 Measurement Technique", Eng Fract Mech, 70, 2003 pp. 417-426.
4. James, M.A., Newman, J.C. Jr.,"The Effect of Crack Tunneling on Crack Growth: Experiments and CTOA Analyses", Eng Fract Mech, 70(3-4), 2003, pp. 457-468.
5. Burton, W., Lease, K.B., Mahmoud, S.H., "The Effect of Measurement Technique on the Experimental Characterization of CTOA-Δa Resistance Curves", Exp Mech, 44(4), 2004, pp. 425-432.
6. Schwalbe, K-H., Newman, J.C. Jr., Shannon J.L. Jr., "Fracture Mechanics Testing on Specimens with Low Constraint – Standardization Activities within ISO and ASTM", Eng Fract Mech, 72, 2005, pp. 557-576.
7. James, M.A., Newman, J.C. Jr., "Characterization of Crack Length Measurement Methods for Flat Fracture with Tunneling", Journal of ASTM International, 2(3), 2005, pp. 31-46.
8. Darcis, Ph.P., McCowan, C.N., Windhoff, H., McColskey, J.D., Siewert, T.A., "Crack Tip Opening Angle Optical Measurement Methods in Five Pipeline Steels", Eng Fract Mech, 75, 2008, pp. 2453-2468.
9. Sakhalkar, S., Frink, E., Mahmoud, S., Lease, K., "CTOA Measurement Methods and Crack Tunneling in 2024-T351 Aluminum", Strain, Vol. 47, Issue Supplement s1, 2011, pp. e130-e141. (DOI: 10.1111/j.1475-1305.2008.00579.x)

10. ASTM Standard E 2472: Standard Test Method for Determination of Resistance to Stable Crack Extension under Low-Constraint Conditions. Annual Book of ASTM Standards, ASTM International, West Conshohocken, PA, 2006.

11. Darcis, Ph.P., McColskey, J.D., McCowan, C.N., Siewert, T.A., "Exploring Methods for Measuring Pipe Weld Toughness", Weld J, 86(6), 2007, pp. 48-50.

12. Darcis, Ph.P., McCowan, C.N., Drexler, E.S., McColskey, J.D., Shtechman, A., Siewert, T.A., "Fracture Toughness Through a Welded Pipeline Section – Crack tip opening criterion", Welding in the World 51(Special Issue), 2007, pp. 225-234.

13. Frink, E., Lease, K., "Characterization of Stable Tearing in Various Metallic Alloys using the CTOA and δ_5 COD Fracture Parameters", 12th International Conference on Fracture Conference Proceedings, Ottawa, Canada, 2009.

14. Hellmann, D., Schwalbe, K-H., "On the Experimental Determination of CTOD Based R-Curves", "Crack tip opening displacement in elastic-plastic fracture mechanics: Proceedings of the Workshop on the CTOD Methodology", K.-H. Schwalbe, Ed., Geesthacht, Germany, 1985, pp 115-132.

15. Hellmann, D., Schwalbe, K-H., "Geometry and Size Effect on J-R and δ-R Curves under Plane Stress Conditions", *Fracture Mechanics: Fifteenth Symposium*, *ASTM STP 833*, R.J. Sanford, Ed., ASTM International, West Conshohoken, PA, pp. 577-605.

16. Mahmoud, S.H., Lease, K.B., "The effect of specimen thickness on the experimental characterization of critical crack tip opening angle in 2024-T351 aluminum alloy", Eng Fract Mech, 70, 2003, pp. 443-456.

17. Newman, J.C. Jr, Dawicke, D.S., Bigelow, C.A., "Finite-element Analyses and Fracture Simulation in Thin-Sheet Aluminum Alloy", NASA TM 107662, Hampton, VA, 1992.

18. Newman, J.C. Jr, James, M.A., Zerbst, U., "A review of the CTOA/CTOD fracture criterion", Eng Fract Mech, 70, 2003, pp. 371-385.

19. Lan, W., Deng, X., Sutton, M.A., "Investigation of crack tunneling in ductile materials", Eng Fract Mech, 77, 2010, pp. 2800-2812.

20. Shivakumar, K.N., Newman, J.C. Jr, “ZIP3D – An elastic and elastic-plastic finite-element analysis program for cracked bodies”, NASA TM 102753, Hampton, VA, 1990.

21. James, M.A., Newman, J.C. Jr, Johnston, W.M. Jr, “Three-dimensional analyses of crack-tip opening angles and δ_5-resistance curves for 2024-T351 aluminum alloy”, *Fatigue and Fracture Mechanics Vol. 32, ASTM STP 1406*, R. Chona, Ed., ASTM International, West Conshohocken, PA, pp. 279-297.

22. Mahmoud, S.H., Lease, K.B., “Two-dimensional and three-dimensional finite element analyses of critical crack tip opening angle in 2024-T351 aluminum angle at four thicknesses”, Eng Fract Mech, 71, pp. 1379-1391.

Chapter 4 – Additional Developments

Introduction

The work described in the previous two chapters/manuscripts represents detailed measurements and analyses of two sets of existing stable tearing data. The work presented there, along with prior Mechanical Testing and Evaluation Laboratory (MTEL) research on surface measurements of CTOA, provide a foundation for an extension of this work which will involve continued investigation of the stable tearing phenomena.

Although not the topic of this thesis document, Frink's doctoral research will investigate the internal (not just surface) aspects of the stable tearing process *in situ* using high energy synchrotron x-ray imaging and diffraction. This investigation will examine aspects such as crack tip blunting, crack initiation, tunneling, and crack tip strain fields. It will involve performing unique stable tearing fracture tests on a specialized beamline at the Advanced Photon Source (APS) at Argonne National Laboratory. In order to transition from the end of the surface measurement work in this thesis into the early stages of Frink's doctoral research, several preliminary items needed to be investigated and determined. Note that the work associated with these preliminary items was performed at MTEL, keeping in mind the goals for APS. Some of the preliminary questions included:

1) What test material(s) should be used at APS?
2) What fracture specimen geometry would be appropriate at APS?
3) What stable tearing tests would be necessary for preliminary surface characterization at MTEL?
4) What is necessary to gain access to the beamline at the APS?

These questions were developed during brainstorming on how to extend our current stable tearing research into the previously mentioned doctoral research, using the APS as the main research tool. Although several other items have been underway during this transition, the remainder of this chapter will provide the current status of the questions listed above.

Material Selection

The material selection process was a three-step process based on three individual factors. Each selection factor narrowed the pool of candidate materials until a specific material was selected, which met all of the requirements. The material for this work was first selected based on attenuation coefficient, which is relevant on the synchrotron beamline. The attenuation coefficient of aluminums coupled with the typical thicknesses (approximately 1 to 6.25 mm [1-4]) for stable tearing specimens matches well with the range of beam energies at APS. The second step required that the material be related to a class of materials with existing stable tearing characterization data available for comparison. Structural aluminums (e.g. 2024-T351, 7075-T6, 5083-H321, etc) have commonly been characterized in stable tearing. The combination of the first two factors makes aluminum alloys fitting candidate materials for surface stable tearing characterization as well as synchrotron *in situ* characterization. Considerations for diffraction made the final selection of the material – a small grain size is required in order to obtain enough grains in the diffraction volume. Thus, a grain refined aluminum alloy was selected which correlated with the previously mentioned factors. Based on these factors, the material chosen was 5083-O aluminum (annealed condition, rolled sheet), which is a superplastic material commonly used for transport and architectural applications. The material was received from Superform USA, with an equiaxed grain size of about 10 microns [5] (compared to 2024-T3 Al rolled sheet, which is anisotropic and has grain sizes on the order of 100 microns in the rolling direction [6]).

Specimen Geometry Selection

In addition to choosing a specimen type for this study, parameters such as material orientation, and specimen size and thickness were also considered. Compact tension (C(T)) laboratory fracture specimens were selected for this work. This type of fracture specimen is well suited for CTOA characterization and is specified in the ASTM standard for CTOA characterization (ASTM E2472 *Standard Test Method for Determination of Resistance to Stable Crack Extension under Low-Constraint Conditions* [7]). Compact tension specimens have been used extensively in the past at MTEL for surface characterization. Note that the C(T) specimens used for stable tearing characterization have large in-plane dimensions relative to their out-of-plane dimension (thickness) in order to achieve the necessary low constraint condition for stable tearing.

Compact tension specimens were fabricated from the 5083-O Al sheets in the T-L orientation, as researchers have shown [8] that in this orientation the 2024-T3 alloy exhibits at least some initial flat fracture during the beginning of the stable tearing process. It is hoped that a similar trend will hold for our selected material. As opposed to slant fracture, flat fracture will simplify the tomographic reconstruction process by providing a more clearly defined and wide open crack to image. In addition, it has been shown [9] that if tunneling does occur during stable tearing, it will occur during the flat fracture mode. Flat fracture and potential tunneling will also make the crack shape more detectable in radiographs and tomographic scans.

The beam energies on beamline 1ID-C at APS (the "specialized" beamline mentioned previously) could well penetrate the typical thicknesses of aluminum stable tearing specimens; however, focusing on thicknesses on the smaller end of the spectrum of typical thicknesses will minimize the complexities in the tomographic reconstructions. It should be noted that "typical" tomography studies involving a crack have the luxury of a specimen (and the area of interest) that fits within the beam size. Because of the requirement for large in-plane dimensions relative to the out-of-plane dimension in order to achieve the low constraint condition that drives the stable tearing phenomenon, it is not possible to shrink the specimen down to fit within the beam (a specimen larger than the beam also increases the complexity of the tomographic reconstruction). Thus, as long as the load capacity of the test frame (at MTEL or APS) is not exceeded, all of the standard (ASTM E2472 [7]) stable tearing C(T) specimen sizes can be considered. Thus, for the transitional work presented here, C(T) specimens fabricated in the T-L orientation, with a thickness B = 1.5 mm and a width W = 152 mm were selected for the specimens fabricated from the 5083-O material. It should also be noted that the 5083-O Al material was provided in 1.5 mm sheet form and was tested in the as-received surface condition. A total of 40 specimens were machined, with 20 set aside for later trips to APS or other testing needs.

Stable Tearing Characterization

In order to develop baseline surface stable tearing characterization data for the 5083-O Al C(T) specimens selected for use at APS, stable tearing tests were performed on a number of the specimens at MTEL. The results from these tests were used for decision-making when moving on to preparation for internal measurements at APS (e.g. amount of stable tearing to produce in

samples to take to APS, amount of tunneling to expect, etc). Of the stable tearing tests performed, two specimens were characterized (one with tunneling measurements). In both cases, the 5083-O aluminum C(T) specimens (B = 1.5 mm, W = 152 mm) were machined to the specifications in ASTM E2472 [7].

CTOA Measurement

Stable tearing tests were performed as described in Chapters 2 and 3. During the stable tearing tests, crack tip images were collected simultaneously with load and crack extension every second (using the setup described in the previous two chapters). Post-processing of the images and measurement of CTOA was performed using Method 1 (described in detail in Ch 2 and 3). Surface crack extension and CTOA measurements were obtained and matched with the corresponding test data (applied load and crack extension).

Note that pre-cracking was performed (R = 0.1) to ensure that the ratio of stress intensity factor range to Young's Modulus ($\Delta K/E$) would be below 0.005 $mm^{1/2}$. However, in most of the tests performed, the final ΔK violated this ratio. This was primarily due to the need to achieve a pre-crack in a timely manner and due to the erratic behavior of this superplastic material. In order to potentially observe the effects of the higher ΔK at the end of pre-cracking, one specimen with a valid $\Delta K/E$ ratio (Specimen 2) and one specimen with a larger $\Delta K/E$ ratio (Specimen 11 – selected because it has the most severe ΔK of the specimens that were tested) were selected for stable tearing characterization in this work.

Figure 4.1 shows the CTOA-Δa curves obtained for the two analyzed specimens using Method 1 (Specimen 2 and Specimen 11). Both specimens transitioned to single slant fracture after only about 2 mm of surface crack extension. As shown in the figure, the typical trend (increase in CTOA to a peak and then decrease to a fairly constant value) is observed in both specimens (see Chapters 2 and 3). Critical CTOA was calculated using the same valid ranges described in Chapters 2 and 3 (note that Δa_{max} is well beyond the Δa for the data collected). The results are shown in Table 4.1. The 5083-O Al exhibits a significantly higher critical CTOA than the heat treated 5083-H321 Al (C(T), W = 50 mm, B = 3 mm, L-T orientation) studied by Heerens and Schodel [10]. They observed a critical CTOA of approximately 5 degrees. Their critical CTOA is similar to the results for 2024-T3 Al (C(T), W = 152 mm, B = 2.3 mm, T-L orientation) [8], which exhibited a CTOA of approximately 4.5 degrees. The standard deviation observed for the

5083-O Al in this work is almost twice that of the standard deviation observed in 5083-H321 Al (C(T), W = 152 mm, B = 3 mm) in the previous chapter.

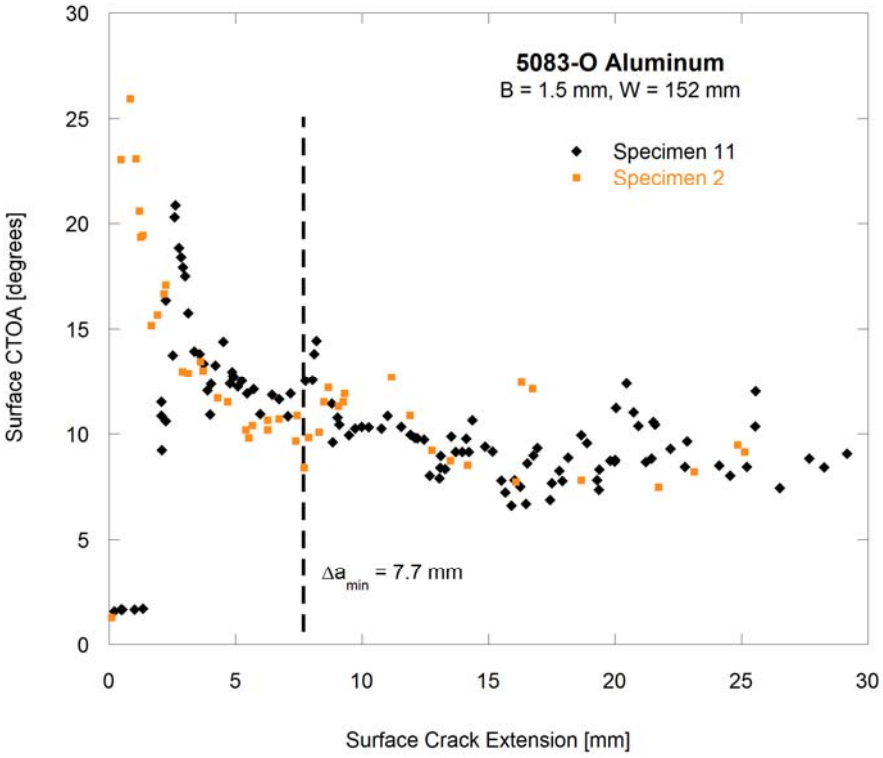

Figure 4.1: CTOA-Δa curves for Specimens 2 and 11

Table 4.1: Critical CTOA and standard deviation results

	Critical CTOA [degrees]	Standard Deviation [degrees]
Specimen 2	10.06	1.75
Specimen 11	9.41	1.56
Average	9.74	1.66

Comparing the results for the two specimens, it seems that the CTOA-Δa curve for Specimen 11 peaks about 1-2 mm later than Specimen 2. However, this is difficult to distinguish due to the scatter in the results. To investigate further, the load-Δa results are shown in Figure 4.2. A more distinguished shift in the results is apparent here. In addition, while analyzing the crack tip

images collected during testing from both specimens, it was noted that the crack tip on Specimen 11 advanced 1-2 mm before blunting and exhibiting the large angle typically observed during stable tearing initiation. On the other hand, Specimen 2 had almost negligible crack extension before blunting occurred. Despite the shift, both specimens reached the same maximum load and had nearly identically behavior after instability. Note that for Specimen 2 the maximum load occurred at approximately $\Delta a = 4.5$ mm, and for Specimen 11 the maximum load occurred at approximately $\Delta a = 7$ mm.

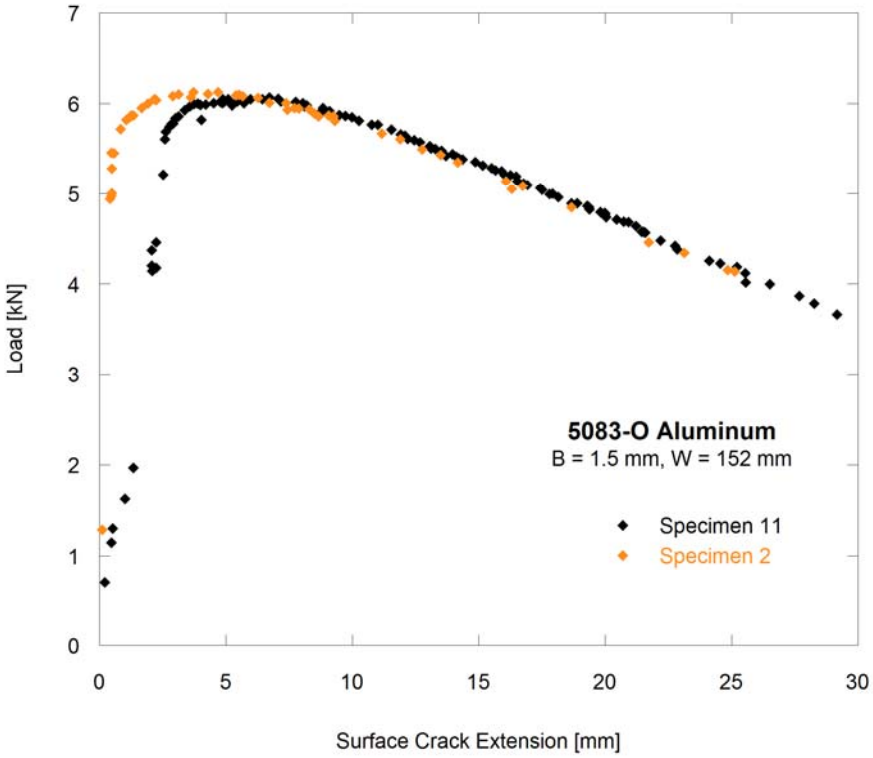

Figure 4.2: Load-Δa curves for Specimens 2 and 11

It is speculated that the slight shift in the load-Δa and CTOA-Δa curves between specimens is observed due to the difference in ΔK at the end of pre-cracking (higher for Specimen 11). The higher ΔK at the end of pre-cracking would have induced a larger plastic zone at the crack tip than Specimen 2 experienced. A plastic zone caused by tensile loading contains compressive residual stresses, which resist blunting and opening of the crack. Therefore, in the case of the larger plastic zone, it makes sense that the crack tip would have had to advance with minimal opening in order to grown through to the other side of the plastic zone. Once out of the plastic

zone, blunting would be able to occur more easily. Calculations of the plastic zone sizes at the end of pre-cracking correlate closely with the amount of crack extension that occurred prior to blunting. However it should be noted that after beginning to tear the specimen, estimates of plastic zone size are no longer valid due to the extent of plasticity. But within the small range of crack extension (and load application), the plastic zone size estimate should be a close indicator.

Tunneling Measurement

Application of marker bands during stable tearing tests is a tool used for observing the tunneling of a crack front, *post mortem*. In this technique, the stable tearing process is stopped, and a number of fatigue cycles are applied to obtain a difference in appearance of the fracture surface. In most cases, this technique is applied in a "multi-specimen" method, where one marker band is applied per specimen at various amounts of stable crack growth to obtain indications of the shape of the tunneled crack. The downside of this is the extensive time required to perform stable tearing on multiple specimens, as well as variations in tunneling between each specimen. However, in Chapter 2 it was shown that a single specimen could be used with multiple marker bands applied and with minimal to no effect on the CTOA response. In this work, marker bands were applied in order to examine the extent of tunneling and determine how to prepare specimens to take to APS (i.e. determine how much surface crack extension they should have prior to going to APS in order to capture what we are after). The general process for applying marker bands was described previously in Chapter 2. More specifically, marker bands were applied as follows (Table 4.2) for a single specimen in this study (Specimen 11):

Table 4.2: Marker band application parameters for Specimen 11

	Just Prior to Application		Marker Band Application (R = 0.7)		
	P_{curr} [kN]	Δa [mm]	P_{max} [kN]	P_{min} [kN]	Cycles
MB1	3.13	1.74	2.55	1.79	3,458
MB2	4.50	2.05	3.59	2.51	2,620
MB3	5.28	2.20	4.24	2.97	2,463

Marker bands were applied at an R-ratio of R = 0.7 and P_{max} was given by 80% of the current load during stable tearing. This factor was introduced in order to ensure that the crack did not suddenly extend a large amount. Cycling was stopped after only a minimal amount of surface crack extension was thought to be observed.

The fracture surface of Specimen 11 is shown in Figure 4.3. The marker bands can be observed, showing slight tunneling for the second and third marker bands. However, the slight tunneling is much less than the expected tunneling. It has been shown by many researchers [11] that the tunneling extent is often maximized after a surface crack extension equal to the specimen thickness, and that the extent of tunneling is equal to the thickness. At the third marker band, the surface crack tip has extended just slightly farther than one thickness, but the tunneling extent is very minimal. After the third marker band, the crack front transitioned into single slant fracture. Researchers have shown that the tunneling extent generally decreases significantly after slant fracture occurs. However, in this case, a significant amount of tunneling was not present prior to the transition to slant fracture. So why was very minimal tunneling observed? Perhaps it is the microstructure – isotropic grains compared to the anisotropic, long grains (in the rolling direction) of the typical materials tested. Maybe this thickness is predominately plane stress, with low resistance to yielding and large amounts of plasticity, and even at mid-plane, near-plane-stress conditions occur.

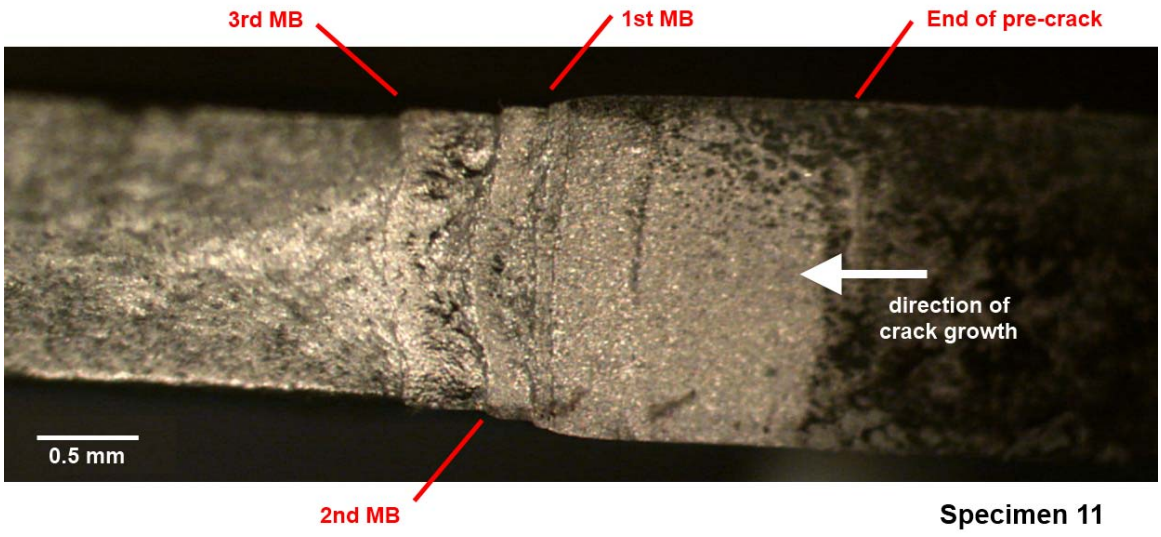

Figure 4.3: Fracture surface of Specimen 11, showing marker bands

Preparation for APS

While characterizing the stable tearing characteristics of 5083-O Al optically at MTEL, a General User Proposal (GUP) with the Advanced Photon Source (APS) at Argonne National Laboratory (ANL) had to be submitted in order to request beamtime (experiment time) on beamline 1-ID-C. Beamline 1-ID-C is equipped with a small hydraulic load frame which allows for *in situ* evaluation. APS is organized into sectors and proposals are submitted to the appropriate group of experts within APS. Beamtime is available in cycles – approximately three months of experiment time followed by two weeks off, back on three months, etc. However, each year the facility is shut down for a month of maintenance. Review of GUPs for the next cycle is performed during the end of current cycle of experiment time. This is a competitive process, and requires a proposal detailing why APS is needed, what the experimental plan entails, how long it will take, etc. Review is based on the technical soundness and probable success of a GUP. If a GUP is turned down during a cycle of review, it can be resubmitted the next cycle, but will not be reviewed again. It will only get a small increase in its score, to help "age" the GUP. If the new score is more competitive with the GUPs in the new round of reviews, then beamtime may be rewarded. If not, resubmission may be required again the next cycle.

In July 2010 we received our first beam time – six days (or 18, eight-hour shifts). This was the first major step in making the transition to internal observation of stable tearing. Note that we obtained preliminary imaging and diffraction data from this visit, but the experimental setup, raw data and analysis are outside the scope of this document.

References

1. James, M.A. and Newman Jr, J.C., "Characterization of Crack Length Measurement Methods for Flat Fracture with Tunneling," *Journal of ASTM International*, March 2005, Vol 2, No 3.
2. Burton, W., Mahmoud, S., Lease, K., "Effects of Measurement Techniques on the Experimental Characterization of Crack Tip Opening Angle-Δa Resistance Curves," *Experimental Mechanics*, 2004, v 44, i 4, pp. 425-32.
3. Dawicke, D.S., Newman Jr., J.C., Bigelow, C.A., "Three-Dimensional CTOA and Constraint Effects During Stable Tearing in a Thin-Sheet Material," Fracture Mechanics: 26th Volume, ASTM STP 1256, Walter G. Reuter, John H. Underwood and James C. Newman, Jr., Eds, American Society for Testing and Materials, Philadelphia, 1995.
4. James, M.A., Newman Jr., J.C., "The effect of crack tunneling on crack growth: experiments and CTOA analyses," *Engineering Fracture Mechanics* 70 (2003) 457-468.
5. Superform USA, Materials Data Sheet, 2011.
6. Mohamed, A., El-Madhoun, Y., Bassim, M.N., "The Effect of Grain Size on Low-Cycle Fatigue Behavior of Al-2024 Polycrystalline Alloy," *Metallurgical and Materials Transactions*, Sep 2004, 35A, 9, pp. 2725-28.
7. ASTM Standard E 2472: Standard Test Method for Determination of Resistance to Stable Crack Extension under Low-Constraint Conditions. Annual Book of ASTM Standards, ASTM International, West Conshohocken, PA, 2006.
8. Newman Jr., J.C. and James, M.A., "A Review of the CTOA/CTOD Fracture Criterion – Why it Works!" AIAA-2001-1324, pp. 1042-1051.
9. Zuo, J., Deng, X., Sutton, M.A., Cheng, C.-S., "Crack Tunneling: Effect of Stress Constraint." *Proceeding of International Mechanical Engineering Congress and Exposition*, Nov 13-20 (2004), Anaheim, CA.
10. Heerens, J., and Schodel, M., "On the determination of crack tip opening angle, CTOA, using light microscopy and d5 measurement technique," *Engineering Fracture Mechanics* 70 (2003) 417-426.

11. Newman Jr., J.C., James, M.A., Zerbst, U. “A review of the CTOA/CTOD fracture criterion,” *Engineering Fracture Mechanics* 70 (2003) 371-385.

Chapter 5 – Conclusion

This thesis presented work in the form of two journal manuscripts with a third chapter containing an overview of continued work in the area. All research was aimed at experimental characterization of the stable tearing fracture phenomenon for metallic materials in low-constraint conditions.

In the first manuscript (Chapter 2), various CTOA measurement methods were employed on 2024-T351 Al. The largest critical CTOA was obtained using Method 1, and the smallest was from Method 3. Method 3 also exhibited the highest standard deviation between the various methods. Marker bands were also applied in order to determine the extent of tunneling. The observed extent of tunneling did not correlate to the extent of tunneling determined from the "apparent crack tip" in Methods 2 and 3. Finally, the computational results for load-Δa did not match the experimental results, without taking into account the extent of tunneling. However, the computational critical CTOA closely matched the experimental critical CTOA from Method 1.

The measurement methods presented in Chapter 2 led into the investigation of the three materials studied in Chapter 3. The second manuscript (Chapter 3) discussed various CTOA measurements employed on three materials. The various effects of material behavior and method behavior were discussed in relation to the CTOA-Δa behavior of each material and method. Method 1 had the highest CTOA for all three materials, while the 2024-T351 Al had a coefficient of variation (COV) almost twice that of the Ti-6Al-4V for all three methods. This was noted to be likely due to the difference in crack shape (meandering versus smooth, respectively). The initial behaviors of the CTOA-Δa curves were linked with the shape of the blunted initiation of the crack – more parallel flanks (Ti-6Al-4V) versus more gradual transition/opening (the two aluminums).

From the surface characterization in Chapters 2 and 3, it becomes apparent that there is a need to further understand the stable tearing phenomenon, perhaps from an internal point of view rather than from the surface. The work presented in Chapter 4 discussed recent work performed to transition from investigations of the surface (as in Chapters 2 and 3) to investigations of internal aspects. From experimental surface CTOA characterization of 5083-O Al (the material selected for this work) higher critical CTOA values were obtained than a 5083-H321 Al, for example. Little tunneling was observed, even before the transition to slant fracture.